Abstract

DANIELS, PATRICK R. High Permittivity Barium Titanate Thin Films. (Under the direction of Professor Jon-Paul Maria.)

As the demand for smaller, faster and more robust electronics increases, the sophistication of system design and the optimization of material properties must improve. In order to accommodate these goals, electrical components, such as capacitors, must be placed closer to the integrated circuit chip and consume less area on a printed wiring board. One approach to this end embeds these passive components into the printed wiring board directly beneath the integrated circuit chip. Previous work at NCSU pioneered a thin film ferroelectric capacitor technology that satisfies the principle demands. This thesis describes a set of advancements to this technology of the thin film dielectrics on flexible copper and platinum foils that target specifically enhanced permittivity through microstructure control.

Barium titanate was deposited on copper and platinum foils by a chemical solution deposition process with the intent of investigating the effects of the A:B site ratio on the microstructure and electrical properties. The primary investigation involved preparing a range of dielectric compositions from 0 to 5% excess barium and annealing them to temperatures ranging from 900 to 1200°C for 20 hours. The annealing atmospheres and maximum temperature limits were chosen with respect to preserving the integrity of the metallic foil substrates.

On Pt substrates, as annealing temperature and the amount of excess barium increased the average grain size increased dramatically. Average grain size grew from 70 nm for a stoichiometric film annealed at 900°C to 800 nm for films with 4% excess barium annealed at 1200°C. The grain size decreased in films with 5% excess barium annealed at 1200°C due to the development of a second phase identified by x-ray diffraction. This data is in sharp contrast to existing descriptions of the $BaTiO_3$ binary phase diagram that suggest ppm levels of solid solubility associated with the $BaTiO_3$ intermediate compound and present interesting new questions regarding stability of Ba excess crystals.

Guided by this Pt substrate reference data, the microstruture – dielectric property relationships were explored for $BaTiO_3$ films on copper foil. Compositions of 1:1 barium titanate and 3% excess barium annealed at 900 and 1060°C were prepared and characterized respectively. The room temperature permittivity increased from 1800 to 4000 with the addition of excess barium and increased annealing temperature. The grain sizes ranged from x1 nm to x2 nm respectively. These results demonstrate a completely new method of controlling grain size in $BaTiO_3$ with Ba excess, and the success of these methods to engineer extrinsic permittivity contributions consistent with well-prepared bulk ceramics.

In addition, thin films of $Ba_{0.7}Sr_{0.3}TiO_3$ were deposited on copper foils via RF magnetron sputtering with the intent of investigating the effects of process flow on the percent yield of working capacitors with respect to electrode size – a second challenge

in the development of a viable embedded high value capacitor technology. In the previously established conventional process, electrode metallization was performed after annealing at 900°C. In the newly developed co-firing process, electrode metallization is performed after sputtering deposition but before annealing at 900°C. By changing the process flow, of the fraction of working 5 mm diameter capacitors increased from 0% to 100%. These capacitors were prepared on copper foils with a dielectric thickness of less than 1 μm in the absence of clean room conditions. A model involving curvature-controlled de-wetting is proposed to explain the success of this method to obviate the short circuits that typically accompany geometric asperities associated with polycrystalline thin films and rough substrates.

High Permittivity Barium Titanate Thin Films

by
Patrick Daniels

A thesis submitted to the Graduate Faculty of
North Carolina State University
in partial fulfillment of the
requirements for the Degree of
Master of Science

Materials Science and Engineering

Raleigh, North Carolina

2008

APPROVED BY:

_____	_____
Nadia El-Masry Professor Materials Science and Engineering	Gerry Lucovsky Professor Physics

_____
Jon-Paul Maria
Associate Professor
Materials Science and Engineering
Chair of Advisory Committee

Biography

Patrick Richard Daniels was born in Elysburg, PA on April 13th of 1984 to Michael and Kathleen Daniels. His older brother Michael had turned two years of age only weeks prior. He and his family spent the next nine years in Elysburg and decided it was time for a change. They moved to Greenville, NC where Patrick would eventually attend Junius H. Rose high school. During his high school career, he played for the baseball team and was the captain of his wrestling team for both Junior and Senior year. After graduation, Patrick decided to pursue an education in the field of Materials Science and Engineering at North Carolina State University. For the first three years of his college life, he worked as a sales associate at Dick's Sporting Goods and then as a Kitchen Supervisor at Damon's Grille. These jobs taught him many invaluable life lessons including the value of a dollar and to perform under pressure. However, the most important lesson Patrick would learn was the value of an education. With senior year came a senior project sponsored by Dupont Microelectronics. This was the avenue through which he came to work as an undergraduate research assistant for Professor Jon-Paul Maria which would make all the difference in the world. Originally Patrick did not intend to continue his education past a bachelor's degree, but the encouragement and advice of Professor Maria eventually won out and he decided to pursue a Master of Science degree. Professor Maria was kind enough to welcome Patrick into his research group where Patrick would work on the development of a thin film capacitor on foil technology. The research went well and he made great friends along the way. He finished his master of science degree in the field of materials science and engineering at NCSU in august of 2008. After that, he took a position as a GaN Crystal Growth Engineer with Kyma Technologies in Research Triangle Park, NC.

Acknowledgements

First and foremost I would like to thank my advisor and good friend, Professor Jon-Paul Maria. Without his constant aid, direction and encouragement, I would not be where I am today. He believed in me even in times when I didn't believe in myself. For this and so much more, I am truly grateful.

I would like to thank everyone in the Electronic Oxides group. Professor Maria was very successful in putting together a group of people who could help and support each other which was a fete from which I often profited and could not imagine doing without. Seymen Aygun and Peter Lam were always willing to help as well as join me for a beer after some persuasion. Michelle Casper and her awesome roommates on several occasions invited us to their place and stuffed us with amazing food. Mark Losego was an amazing asset given his vast knowledge of all things science.

I would also like to say thank you to those outside the group who offered a helping hand and their support. Jon Ihlefeld, a former member of the group, would respond to email inquiries within minutes at almost any hour of the day. Jess Jur was always willing to offer his knowledge as well as join us at Bojangle's. James Tweedie and Tony Rice shared their expertise in XRD and were always good for a few laughs anytime of the day.

However, the most important people in my life are without a doubt my parents, Mike and Kathy Daniels, and my brother Mike Daniels. Without their support and guidance throughout my life, I would not be where I am today. They have always been there for me and I could not imagine having a better family. Thank you with all of my heart.

Table Of Contents

List of Figures

Chapter 1: Introduction

This thesis focuses on the development of a thin film capacitor on foil technology for embedded passives made possible through a collaboration of research efforts by Dupont and North Carolina State University. This thesis represents an extension of a previous NCSU-DuPont collaboration initiated in 2002, which now focuses on composition effects that influence the dielectric response of thin film barium titanate, and novel methods for achieving large area capacitors without clean room processing. The following survey of literature summarizes the most pertinent scientific publications that build a framework in which the experimental results can be discussed and interpreted.

1.1 Embeded Passive Components

The ever-present desire for smaller and faster electronics led to the idea of embedded capacitors. A thin film capacitor on metallic foil substrate technology could be developed to replace the existing bulk ceramic inter-digitated capacitors on printed wiring boards. The 2-D thin film capacitors could be embedded directly beneath the integrated circuit chip rather than be spread out across the printed wiring board and

surface mounted as are conventional 3-D bulk ceramic capacitors. This would decrease the amount of area the printed wiring board requires as well as improve device speed and performance as these properties are directly related to the distance between the capacitor and the integrated circuit chip. A diagram of the proposed geometry can be found in figure 1.1.

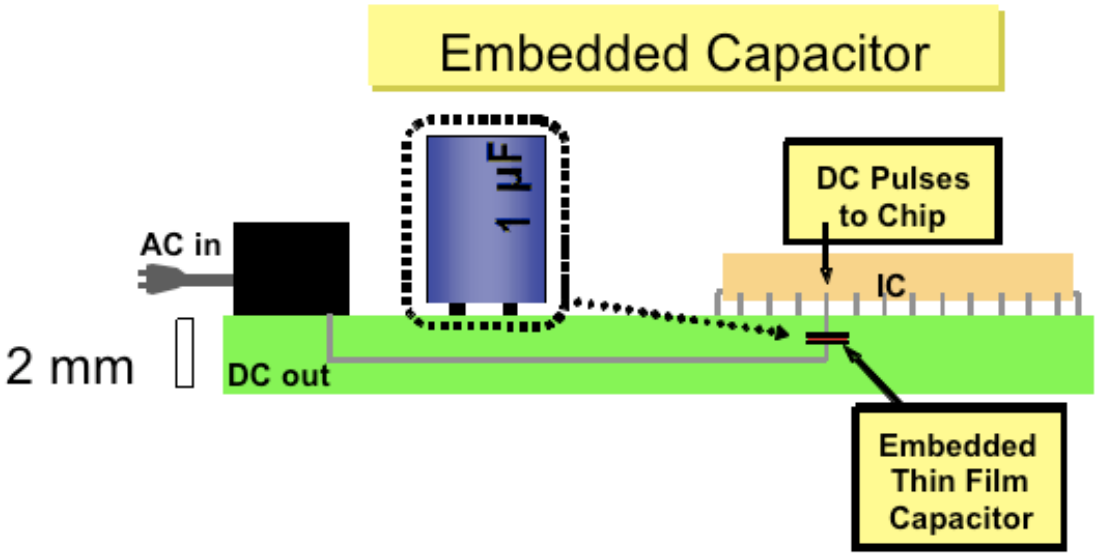

Figure 1.1: A schematic representation of a proposed thin film capacitor technology that will replace conventional interdigitated bulk ceramic capacitors.

The embedded thin film geometry has several advantages: 1) inductive loss is reduced by decreasing the lead length since as is illustrated in figure 1.1 the embedded capacitor can be located directly below the IC in/out connections [1,2] 2.) Processing becomes more efficient by allowing lithographic patterning, lamination assembly, and parallel integration as opposed to the commonly used "pick and place" process 3.) a

reduction in lead containing solder joints[3]. The problem associated with the development of this technology is reaching the commercially desired capacitance density of 5 μF/cm^2 [1]. Previous technologies such as lead zirconate titanate thin films and $BaTiO_3$ dispersed in BaO glass have not rendered a capacitance density above 0.5 μF/cm^2 [1,4]. Thus, a thin film capacitor technology has not yet been developed that would satisfactorily replace current bulk ceramic capacitors of all capacitance values used in modern electronic packages. To be cost effective, the same technology needs to satisfy all capacitor needs.

1.2 Size Effects in Bulk Barium Titanate

Ultimately, it is the large permittivity of ferroelectric crystals that make them interesting for embedded capacitor components. In bulk, permittivity values can exceed 10,000, thus the target capacitance density can surpass 5 μF/cm2 while maintaining layer thicknesses greater than 1 μm. However, as the following section indicates, achieving bulk capacitor values in very fine crystals or very thin layers presents a long standing challenge with both scientific and technological aspects.

It has been shown that the permittivity, domain size, and the temperature dependence of the crystalline phase of ceramic barium titanate are dependent on the average grain size of the dielectric [5-7]. Room temperature permittivities for polycrystalline materials can range from 400 to 6000 depending on the grain size and

crystallinity of the dielectric. To establish a frame of reference for comparison the room temperature a-axis and c-axis permittivities for single crystal barium titanate are 4000 and 400 respectively[8].

Arlt *et al*. published a landmark paper that summarized grain size effects in ceramic $BaTiO_3$ in 1985 [5]. Arlt and coworkers prepared a sample set of barium titanate with grain sizes ranging from 0.3 to 50 μm in order to characterize the effect of grain size on permittivity. It was found that permittivity reaches a maximum as grain size is increased from 0.3 to 1 μm, above which permittivity drops dramatically [5]. The increase in permittivity observed as grain size is decreased from 100 to 1 μm is attributed to an increase in domain wall density within each grain. Arlt observed that domain width scaled as the square root of grain size. Since the motion of domain walls under small field excitation is the origin of large permittivity in $BaTiO_3$, an increase in their volume density magnifies the extrinsic contribution to permittivity. The decrease in permittivity observed as grain size decreases from 1 to 0.3 μm was explained by TEM studies that found a reduction of domain walls in sub 0.7 micron grains, and few to no 90° domain walls. The inability to form 90° domain walls removed the materials ability to accommodate strain from the ferroelectric phase transition, which is believed to cause a reduction of tetragonality, and ultimately permittivity. The internal stress model of Bell explains these observations, and for many years, it was believed that fundamental, thus unavoidable decreases in permittivity occurred in $BaTiO_3$ thin films,

and provided a major limitation to dielectric applications needing both small dielectric thickness and large permittivity [9]

Approximately 12 years later, Frey *et al*. revisited the work done by Arlt *et al*. and showed that unlike previous conclusions, sub-micron grains of barium titanate can exhibit permittivity values in excess of 4000 [10]. Aided by the technological advances of processing science, Frey and Payne were able to prepare extremely dense and fine grained $BaTiO_3$ ceramics using a combination of advanced powder synthesis and high pressure sintering techniques. Fine-grained barium titanate was examined for grain sizes from 1.7 μm down to 70 nm. It was found that the permittivity decreased as grain size decreased, but permittivities in excess of 2000 were measured in grain sizes below 100 nm [10]. This is a critically important result since it shows that previous investigations observed size effects, but these effects were not intrinsic to the material. The decrease in permittivity found in Frey and Payne's work is attributed to a series dielectric mixing effect that becomes more important as the grain surface area to grain volume ratio increases [10]. Frey and Payne developed the brick wall model where each ferroelectric grain contained a high permittivity core, the brick, and a low permittivity grain boundary, the mortar. TEM would show that a crystallographically disordered grain boundary layer with presumably low permittivty occupied approximately 0.1 nm of the outermost layer of each grain [10]. Thus, it was the improved ability to process fine ceramics with thin and clean grain boundaries that enabled bulk Permittivities to be achieved in crystallite sizes below 100 nm. The implications of this work are

straight forward in the context of this thesis: At grain sizes where ceramic $BaTiO_3$ is useful in micron-thick film applications (around 300 nm), permittivity values in excess of 4000 are achievable. It is only a matter of advancing the science of thin film processing to achieve the needed homogeneity and perfection of microstructure.

1.3 Challenges of Processing Thin Film Barium Titanate

Size effects of barium titanate are particularly important when dealing with thin films due to the inherent challenge of growing large grained material. The difficulty of grain growth in the thin film geometry is due mainly to the practical limitations of thermal budget. Annealing temperatures comparable to bulk barium titanate are difficult to achieve for thin films because they are often limited by the substrate. A rigid substrate with a different thermal expansion coefficient than that of barium titanate will result in increasing stress in the dielectric thin film as temperature is increased [11,12]. This thermal stress will often lead to cracking and chipping of the thin film at temperatures exceeding 900°C. In comparison, sintering temperatures for bulk barium titanate, which is a highly refractory ceramic oxide, are in the range of 1300 °C. Since thin film processing temperatures, especially on rigid substrates, are limited to ~ one half of this value, the ability to achieve full density and perfect crystallinity will be compromised. Generally speaking, full density can be achieved using a variety of thin film processes, however, grain sizes are routinely limited to the 100 to 300 nm range.

Ihlefeld *et al.* showed that $BaTiO_3$ grain sizes exceeding 5 μm could be achieved at 900°C in barium titanate thin films using a barium borate fluxed chemical solution deposition process [13]. In this case the presence of a liquid phase flux assisted in the mass transport during crystallization and densification, thus the ability to grow large grains with a high degree of structural perfection. The measured room temperature permittivity for such films exceeded 3000 and x-ray diffraction revealed peak splitting indicative of tetragonal symmetry. This study of borate-based fluxing demonstrated that microstructure engineering is possible through chemistry, and this work, to a large extent inspired the experimental plan of this thesis.

1.4 Compositional Effects of Barium Titanate

The barium titanate equilibrium phase diagram has been extensively explored for bulk materials, and though the original phase diagram was prepared in 1953 by Rase and Roy [14], there remains debate regarding the issues of solubility at the 1:1 BaO-TiO_2 intermediate phase.

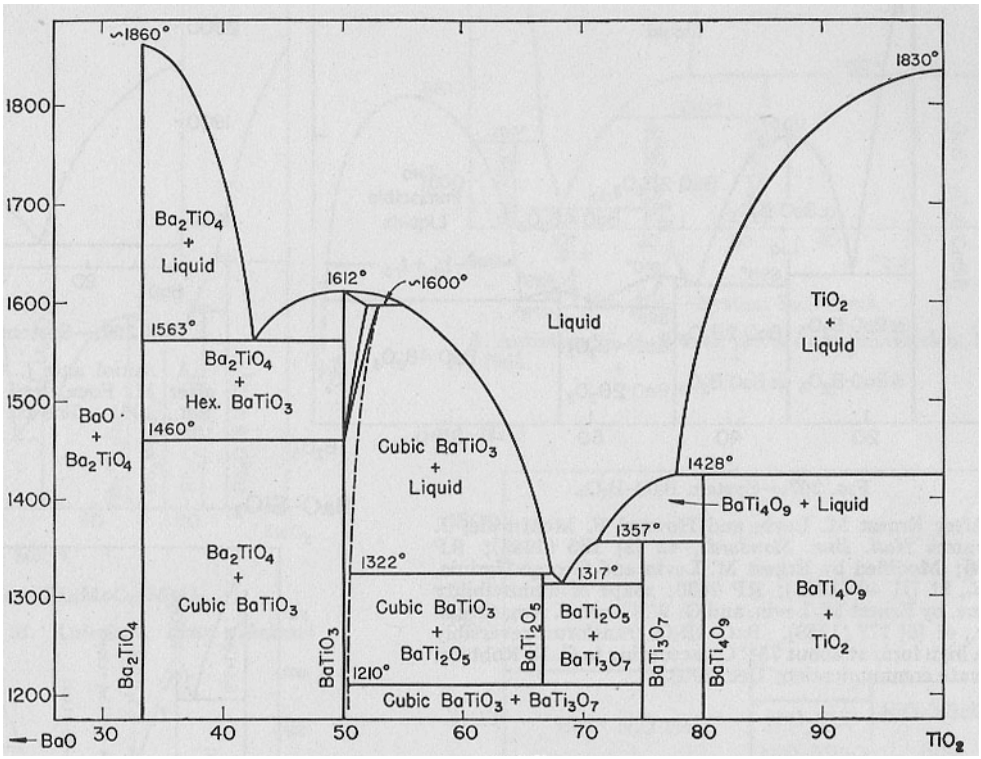

Figure 1.2: $BaTiO_3$ phase diagram developed by D.E. Rase and Rustum Roy

Historically, the first detailed examination of phase field width in $BaTiO_3$ was conducted by the Smyth group at Lehigh University through a series of investigations involving the Ba-rich and Ti-rich sides of the diagram, Smyth *et al*. established a solubility limit of 100 ppm BaO excess in bulk $BaTiO_3$ and the presence of the barium rich Ba_2TiO_4 phase when samples with greater BaO excess compositions were annealed above 1000°C [15]. Smyth *et al*. also established a limit of 100 ppm TiO_2 excess in bulk $BaTiO_3$ at 1100°C where the titanium rich $Ba_6Ti_{17}O_{40}$ phase nucleated.

Generally speaking, the Lehigh results established the following phase diagram detail for $BaTiO_3$ and this data was widely considered to complete the understanding of

stoichiometry effects, and was used to guide solid state processing of $BaTiO_3$ powders and ceramics (and to a large extent the entire multilayer $BaTiO_3$ capacitor industry) for many years. It is noted, however, that much of the evidence for solubility was based on scanning electron microscopy that by today's standards exhibited rather low resolution.

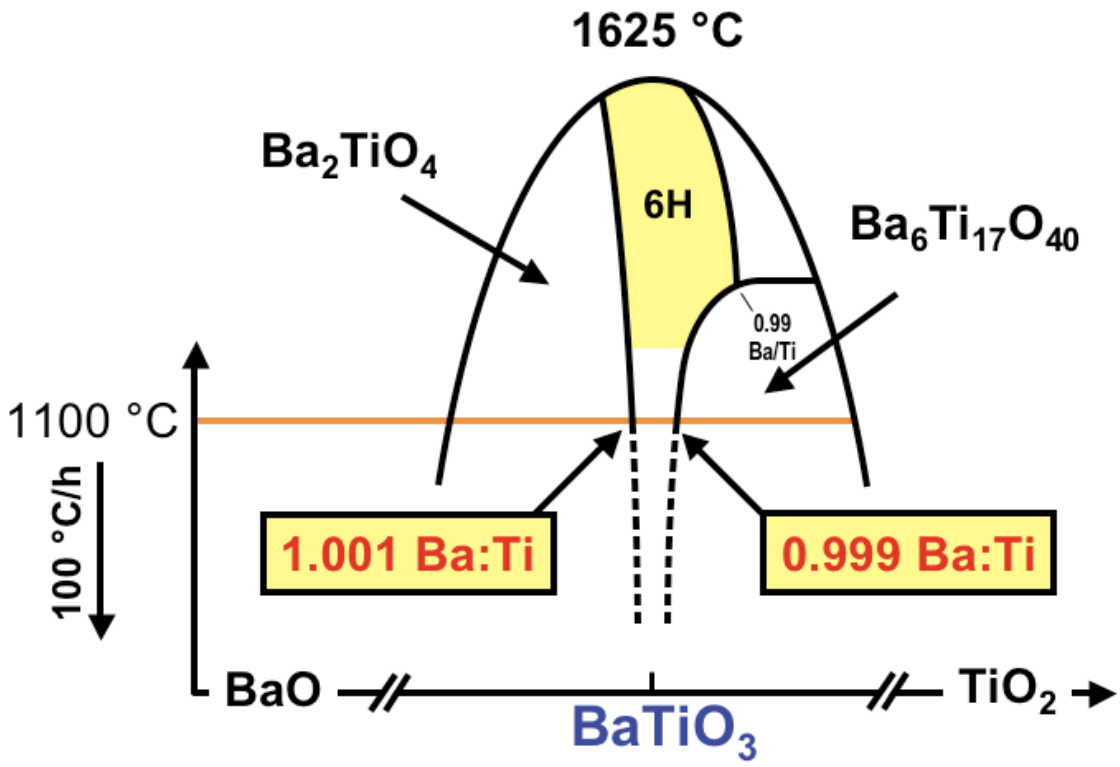

Figure 1.3. The barium titanate equilibrium phase diagram interpolated from the work of Hu, Lee and Sharma

More recently, The Randall group of Penn State University revisited the $BaTiO_3$ phase diagram. The motivations were associated with a curiosity regarding the phase fields under low oxygen partial pressures. Between the time of the original Lehigh work and the present day, the industry standard procedure for barium titanate

capacitors switched from noble metal to base metal electrodes. Consequently, firing conditions were changed from normal atmospheric conditions, to forming gas and nitrogen mixtures that produce oxygen partial pressures below 10^{-10} atm pO_2. It is conceivable that the change in defect chemistry that such firing conditions can produce will also influence phase stability. This technology change warranted a more detailed investigation.

Randall *et al.* performed this in depth study of the effects of oxygen vacancies in barium titanate using differential scanning calorimetry. This represents a novel means of resolving the barium titanate phase field and for bulk samples, has produced a much higher "resolution" phase diagram. Effectively the Randall group relied on the fact that the $BaTiO_3$ primary phase transition temperature is first order, thus with compositional variation, the transition temperature will vary smoothly, and experience a discontinuity when a phase boundary is reached. Since DSC methods can detect phase transitions with great accuracy, this is an excellent means of evaluating phase fields in $BaTiO_3$. The first important finding in this work was that at 1473K an annealing time of 30 hours was required to reach equilibrium – this cast some doubt as to weather many of the previous studies had measured samples that were at thermodynamic equilibrium [16]. The second important finding in this work was that the solubility of Ba and Ti in barium titanate spans a wider range than previously believed.

It was shown previously by Hardlt *et al.* that the curie temperature of barium titanate decreases as the amount of oxygen vacancies increase. This study was

performed by annealing in highly reducing atmospheres and quenching to establish oxygen stoichiometry [17]. With this information in mind, one can use the phase transition to estimate oxygen stoichiometry and consequently phase stability. Consequently, the overall defect chemistry and its relation to cation stoichiometry must be considered. Randall *et al*. controlled the amount of oxygen vacancies when varying the A to B site ratio. The A to B site ratio can be expressed as (1+δ):1 where positive δ is barium rich and negative δ is titanium rich. The stoichiometry can then be expressed as $Ba_{1-\delta}TiO_{3-\delta}$ and $BaTi_{1+\delta}O_{3+2\delta}$ for barium rich and titanium rich respectively. The term δ is now directly related to the amount of oxygen vacancies and the composition of the film. As the magnitude of δ increases the number of oxygen vacancies will increase following the degree of deviation from stoichiometry since in $BaTIO_3$, $A:B \neq 1$ manifests in cation vacancies that are compensated by vacant oxygen sites. Therefore as the magnitude of δ increases the curie temperature of the dielectric will decrease as the number of oxygen vacancies increases until a stoichiometry is reached in which a second phase is able to precipitate. In this situation, further deviations from stoichiometry would not produce a change in Curie temperature since these compositional variations would produce an increasing quantity of second phase (which is a linear dielectric regardless of the sign of δ). Randall *et al*. used this relationship and experimentally measured property trends to determine the barium titanate solubility window by monitoring the Curie temperature as a function of A:B in $BaTiO_3$ powders. It was determined by this method that the solubility window of barium

titanate spans the A to B site ratio from 1.005 to 0.98 [18]. This window is much larger than previously believed.

Generally speaking, there are very few reports of electrical property dependencies on composition in $BaTiO_3$. This is due primarily to the narrow phase field, and that the neighboring phases, on either side of the perovskite phase are non-ferroelectric with low permittivity values. Adding any quantity of second phase will only serve to dilute the non-linear dielectric response that makes $BaTiO_3$ a useful dielectric. The effects of the Ba-rich Ba_2TiO_4 phase on the dielectric properties and the microstructure of barium titanate were examined by Beauger *et al*. It was found that the presence of the orthotitanate phase decreased room temperature permittivity and increased tan δ values [19]. The second phase was also found to be a grain growth inhibitor. While these effects were seen with all compositions, it was determined that the detrimental effects of the second phase were severe in compositions exceeding 2% Ba_2TiO_4 by volume. Despite the thoroughness of Randall's equilibrium investigations, the dielectric properties were not reported.

1.5 Composition Effects in Barium Titanate Thin Films

Though there are numerous reports of composition effects on the dielectric properties of $BaTiO_3$ and more commonly $(Ba,Sr)TiO_3$ (BST) thin films, these are of limited use in understanding the structure-property relationships that regulate the

dielectric response [20,21]. Most studies discuss MOCVD deposited materials in the vicinity of 650 °C, and correspond to films that are far from equilibrium. Arguably, Streiffer *et al* conducted the most sophisticated investigation of A-site to B-site ratio effects in BST. He determined an optimal composition that was not stoichiometric, however, this optimum was based on a number of parameters germane to the application of embedded dynamic random access memories [22]. In summary, the thin film community observed much higher solubility for the BST system, however, the low temperature synthesis, the presence of residual organics, the comparatively poor crystallinity, and the ultra-fine grain size all contribute to extrinsic mechanisms that produce apparent solubility [23].

1.6 Chemical Solution Deposition of Barium Titanate Thin Films

A chemical solution deposition technique often referred to as sol-gel has been used to deposit thin films of complex oxide materials for more than one hundred years. The technique has many advantages over solid-state bulk processing. Because the film is created from chemical pre-cursor solutions, higher purities and more precise stoichiometries can be achieved than in bulk processes due to the availability of ultra-high purity chemicals that are dissolved and mixed in solution. However, one of the drawbacks to this technique is that often dangerous and atmosphere-unstable chemicals are used during preparation.

The most common of the chemical solution (or CSD) techniques are sol-gel processes, hybrid-chelate processes and metal-organic decomposition. Sol-gel processes are based on using alcohols as both solvents and reactants; hybrid-chelate processes stabilize solution components by modifying ligands present in the source chemical, while metal-organic processes employ chemical constituents that do not react with water.

Sol-gel and hybrid-chelate processes are very similar and for this reason can easily be confused. Both processes start with metal-alkoxides which are then reacted to stabilize them in the presence of water. The difference lies in which solution component chelates the metal-alkoxide and which solution component dissolves the metal precursor. Sol-gel processes employ only alcohols such as methanol or 2-methoxyethanol as chelating agent and/or solvent. Hybrid-chelate processes often use acids such as acetic or citric acid as the solvent and chelating agent. While the hybrid-chelate process is more resistant to moisture than its alcohol based sol-gel counterpart, the complexity of the present chemicals results in continuous, and often, unexpected reactions. A sol-gel chemistry will often remain stable far longer than a hybrid-chelate chemistry that is prone to precipitation after a period of time.

Metal-organic deposition differs from sol-gel and hybrid-chelate processes in that the chemicals chosen for metal-organic deposition often contain large carboxylate groups which make them very stable in the presence of water. This is the least common of the three methods due to its susceptibility to cracking during pyrolysis

when the large carboxylate groups are removed. The large ligands are removed from the film during pyrolysis and cause cracking as a result of large weight loss and shrinkage that occurs [24]. This can partially be overcome by using starting reactants with smaller ligands.

The process of depositing barium titanate thin films by CSD has been in development for many years. Schwartz *et al*. was the first to develop a hybrid-chelate chemistry and identify the barium titanate crystallization temperature of 590°C [24]. In this work, barium acetate was dissolved in acetic acid and titanium butoxide was added to the solution. Siegal *et al*. developed a chemical solution deposition process for producing thin films of strontium titanate on nickel foils. The process was comprised of two precursor solutions: A-site) Sr-acetate dissolved in glacial acetic acid. B-site) Ti-isopropoxide chelated with Acetylacetone. The chelation of the Ti-isopropoxide with acetylacetone decreases the reactivity of the Ti-isopropoxide and slows hydrolysis [25]. A similar process could be developed for the preparation of Barium Titanate given the identical Ti precursor.

Hoffmann *et al.* did a study on the effects of chemical precursors on the morphology of barium strontium titanate films on prepared by CSD. In this study, the titanium precursor used was always Ti-tetra-*n*-butoxide and the barium and strontium sources examined contained different length alkyl chains such as; acetates, propionates and 2-ethyl-hexanoates [26]. It was found that the length of alkyl chain influenced the decomposition temperature of the film as longer chains decompose at lower

temperatures. The low temperature decomposing carboxylates exhibited a fine grained and randomly oriented morphology whereas the high temperature decomposing carboxylates resulted in columnar growth. It was also shown that decreasing the molarity of the solution aided the transition from growing randomly oriented films to films with a columnar morphology [26].

Chapter 2: Experimental Procedure

In this chapter, two experimental procedures developed to achieve the technology goals for the barium titanate thin film capacitor on metallic foil technology are explained. Experiments with the aim of increasing the permittivity of the barium titanate thin film were based on a sol-gel and spin casting technique developed previously by Dr. Jon F. Ihlefeld. This technique was chosen due to its inherent ease of controlling the chemical composition. Experiments with the aim of achieving large-area thin film capacitors were performed using a barium titanate sputtering technique developed previously by Dr. Brian J. Laughlin. This sputtering method was chosen for these large area experiments due to the more uniform microstructure as compared to sol-gel prepared material.

2.1 Chemical Solution Deposition (CSD)

CSD synthesis of $BaTiO_3$ begins with the preparation of two separate pre-cursor solutions: one solution contains the A-site atoms (in this case Ba) and the other contains the B-site atoms (in this case Ti). Solutions are prepared in a glove box that is flushed with dry nitrogen to keep the humidity below 15% to minimize the interactions between raw source chemicals and water vapor. Precision and accuracy of solution molarity is maximized by massing all components on a Mettler-Toledo AT201 5-decimal digital balance that is accurate to 0.1 milligrams.

The A-site solution, which is the barium source, is prepared by dissolving barium acetate (99% Sigma-Aldrich) in glacial acetic acid (99.99% Sigma-Aldrich). After placing a piece of weigh paper on the balance and zeroing the scale, barium acetate is massed out as close to the desired mass of 3 grams (0.012 equivalent moles) as possible and the actual mass is recorded. Typically, the deviations from the 3 gram target are in the range of 1 mg. The barium acetate is then transferred to a clean Erlenmeyer flask and the weigh paper is massed again to determine the amount of barium acetate that did not get transferred to the flask. This amount is then subtracted from the mass of barium acetate before the transfer.

Next, a magnetic stir bar is placed in the flask containing the barium acetate and all three components are placed on the balance. After zeroing the balance, as close to 25.5 grams or 0.4 moles of acetic acid are added to the flask and the actual mass added is recorded. Typically, the deviations from the 25.5 gram target are in the range of 1 mg. Again, typical deviations are in the range of 1 mg. The mixture is then placed on a stirring plate and stirred overnight to ensure the barium acetate is fully dissolved. The target A-site solution final molarity is 0.5 molar.

The B-site solution, which is the titanium source, is prepared by the chelation of titanium(IV)-isopropoxide with acetylacetone and diethanolamine. A clean Erlynmeyer flask containing a magnetic stir bar is placed on the balance and the scale is zeroed. As close to 2.024 grams or 0.02 moles of acetylacetone is added to the flask. Typically, the deviations from the 2.024 gram target are in the range of 1 mg. The

actual mass is recorded and the scale is zeroed again. Then as close to 0.01 moles of of titanium(IV)isopropoxide (99.999% Sigma Aldrich) which corresponds to 2.844 grams is added to the flask. Typically, the deviations from the 2.844 gram target are in the range of 1 mg. The actual mass is recorded and the flask is zeroed again. Next, as close to 0.268 grams or 0.0025 moles of diethanolamine is added to the flask and the actual mass is recorded. Typically, the deviations from the 0.268 gram target are in the range of 1 mg. The mixture is then placed on the stir plate overnight to ensure the complete chelation of the titanium isopropoxide. The B-site solution final target molarity is 1.8 molar.

The exact molarities of the A-site and B-site solution are calculated. With this information, aliquot quantities of each can be mixed, and final solution can be easily formed with a cation stoichiometry that is accurately known to within 0.1 mol % [27]. This method is ideally suited for preparing sets of solutions with Ba concentrations that are close to ideally stoichiometric, and those with 1, 2, 3, 4 and 5% excess barium. Once the desired stoichiometry is reached the solution is stirred over night to ensure complete mixing and is ready for deposition.

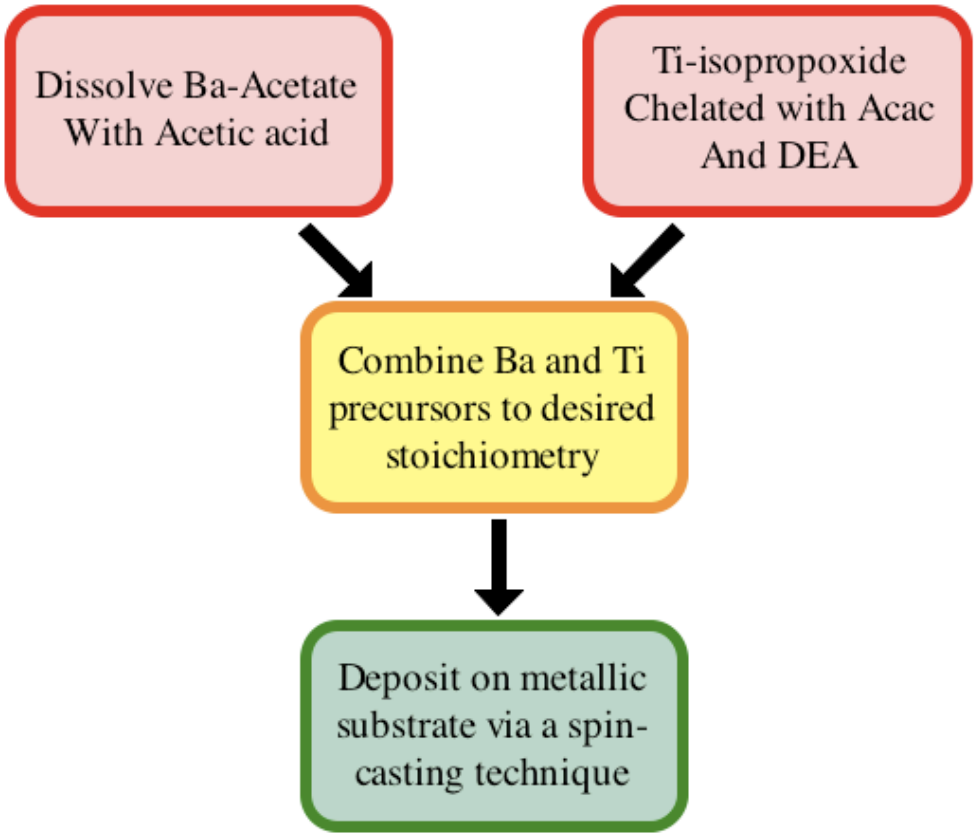

Figure 2.1: Process flow diagram for the preparation of a Ba and Ti solution from precursor solutions.

2.2 Thin Film Formation

$BaTiO_3$ thin films are formed by spin coating the final metalorganic precursor solution on copper or platinum foil substrates. The Cu and Pt foils are 15 and 40 microns and are the preferred substrate for the target commercial technology, however, platinum foils were also used due to platinum's high melting temperature and resistance to oxidation. Due to the expense, Pt foils are reused multiple times. The

dielectric is removed by etching with a 10% hydrofluoric acid solution. The foils are then rinsed twice with deionized water and finally rinsed with methanol and allowed to dry in air to remove surface contaminants.

The first step in deposition is to cut the foil substrate to a manageable size, in this case, approximately 2 inches by 2 inches for copper and 1 cm by 1 cm pieces for platinum. The foil is then taped, along two opposite edges, to a round 3" diameter fused silica substrate which is placed on a Cookson Electronics P-6000 spin coater chuck and secured by vacuum. Prior to spinning, the surface of the foil is completely covered with the final solution by dripping the solution on the foil from a 3 ml Becton-Dickinson syringe that employs a 0.2 micron filter (Fisher Scientific). The foil is spun for 30 seconds at 3000 rpm. The substrate is immediately removed from the spin coater and glass mount and placed directly onto the surface of a 250 °C Mirak Thermolyne hotplate for 5 minutes for solvent evaporation and initial gel formation. This process, which can be seen in figure 2.2, is repeated several times to reach the desired film thickness. Each spun-on layer produces approximately 100 nm of crystallized $BaTiO_3$ film. For these experiments, the process was repeated 6 times for a target final film thickness between 600 and 700 nm.

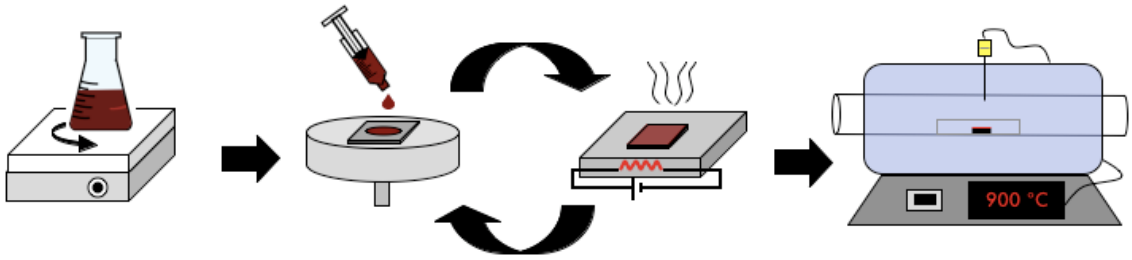

Figure 2.2: A diagram depicting the sol-gel process from start to finish. The metal-organic solution is prepared then spun and dried on the substrate multiple times before the final anneal

2.3 Sputtering Barium Strontium Titanate on Copper Foils

Thin films of barium strontium titanate were also prepared on copper foil substrates via RF magnetron sputtering. A 4 inch diameter sputtering source target was prepared by Super Conductor Materials, INC. with a composition of $Ba_{0.7}Sr_{0.3}TiO_3$. The target was placed in a 4 inch Torus® RF magnetron sputtering source. The source was mounted in a UHV chamber 8 cm above the substrate and tilted 25° off the normal of the substrate. The vacuum chamber geometry can be seen in figure 2.3. This offset off-axis geometry is used to mitigate the effects of anion resputtering and to maximize thickness uniformity. A more detailed description of this sputtering process can be found in the Ph.D. dissertation of Dr. Brian J. Laughlin [28].

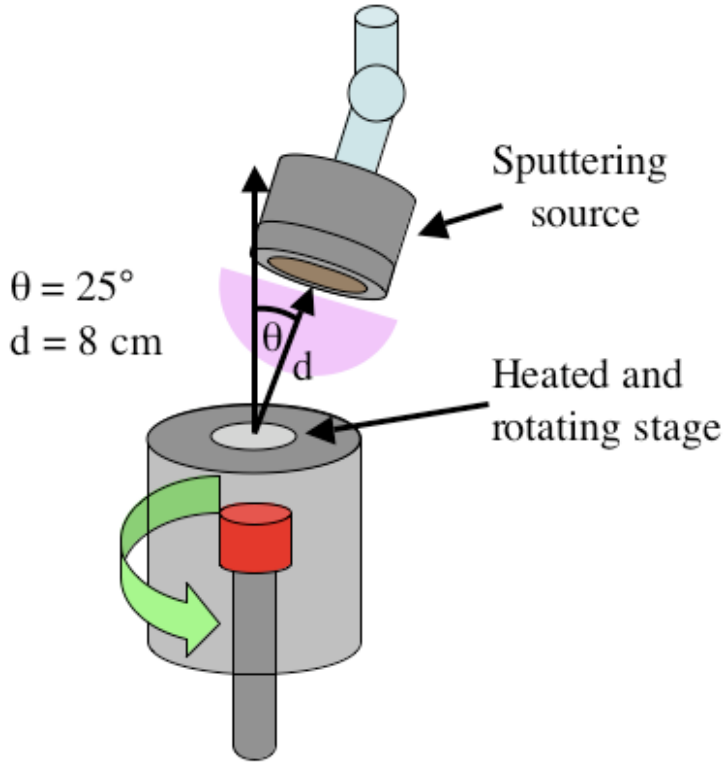

Figure 2.3: The internal geometry of the UHV chamber used for sputter deposition of $BaTiO_3$ on thin metallic foils.

Copper foils were mounted in the sputtering chamber using rectangular brackets with two sizes: 1 inch by 2 inches and 4 inches by 4 inches. The brackets consisted of two metal frames that could be joined with machine screws to clamp the foil and hold it flat during deposition. Figure 2.4 shows pictures of each frame loaded with foil substrates. The frames were constructed of either stainless steel or aluminum. Once a substrate was mounted the frame-foil assembly was placed on top of a stainless steel plate that covered a BN coated graphite heating element inside the rotating

manipulator stage. Due to the thickness of the substrate mounting brackets (1/8 inch), the foil substrate was not in direct contact with the sample stage.

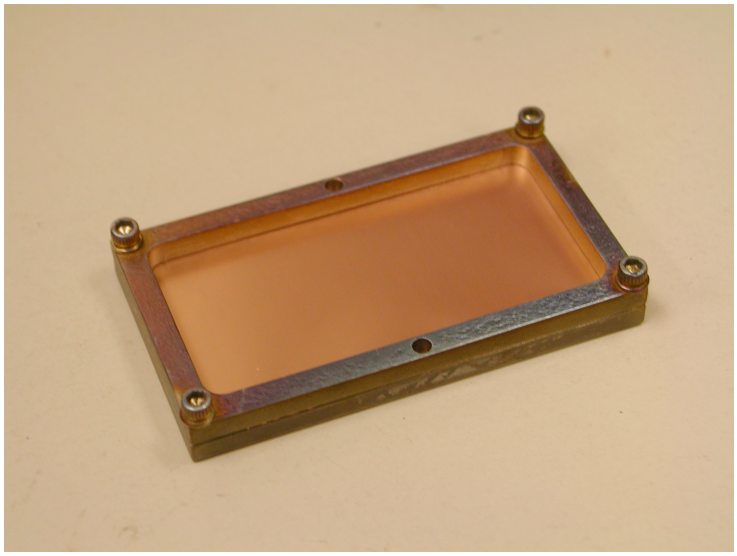

Figure 2.4: A digital photo showing a copper foil substrate affixed in a titanium mounting bracket secured by machine screws.

After chamber evacuation and reaching the target background pressure of 10^{-5} torr, the substrate manipulator is heated to 130 °C from room temperature at a rate of 15 °C per minute. This temperature was chosen as it corresponds to the maximum stage temperature possible prior to rapid oxidation of the copper foil during BST deposition. This deposition temperature refers to the temperature recorded by a thermocouple positioned away from the heater element approximately the same distance as the manipulator stage. Once the temperature stabilized a flow of 20 sccm of 99.99% argon is introduced by a mass flow controller and the pressure is adjusted to 10 mtorr by limiting conduction to the turbo pump by partially closing the gate valve. The

substrate is then rotated at a rate of 5 rpm. Next a plasma is initiated by applying 300 watts of RF power (Advanced Energy RFX 600) to the magnetron source. Optimization of deposition conditions was not the focus of this study. The conditions used are based on the process optimizations conducted in the Ph.D. theses of Laughlin and Ghosh, which used the same sputtering instrument [29,30]. These conditions result in a deposition rate of approximately 1.1 nm per minute. The deposition was maintained for 90 minutes which resulted in a film thickness of approximately 1 micron.

One of the problems experienced with this process was the long term durability of the BST source targets. Non-uniformity and inhomogeneities in the sputtering sources have been known to lead to preferential sputtering. Some locations experience a faster rate of erosion which can lead to pitting and eventual cracking of the source. When a crack occurs, it can act as a charge concentrator and electrical arching is likely. The large amount of energy released during an arching event can damage the target further and cause particulates to come off of the target. These particulates can then be incorporated into the sputtered thin film.

2.4 Annealing of CSD Films on Cu and Pt films

Films on platinum foils fired in an open-air furnace where the sample is placed in an alumina crucible and slid into the hot zone at a starting temperature of 150°C. The furnace is then ramped to the desired annealing temperature at a rate of 30 °C per

minute and left to dwell at temperature for 20 hours. When the dwell time is reached, the furnace is turned off and allowed to cool per Newtonian cooling. The sample is then removed once the temperature has fallen below 150°C.

Films on copper foil are annealed with the same temperature profile as the films on platinum but in a controlled atmosphere tube furnace and a fused silica crucible.

The pO_2 processing window for barium titanate can be seen in figure 2.4. In order to reach the pO_2 range where oxidation of the copper substrate could be avoided without decomposition of the dielectric film, a controlled low pO_2 atmosphere is needed. A Lindberg-Blue M tube furnace using a 2" outer diameter fused silica tube and Viton o-ring sealed endcaps was used to achieve the needed atmospheric conditions. The furnace geometry can be seen in Figure 2.5. Each end cap had a Swagelok gas port that was connected to an H_2O bubbler. Process gases were fed through the first bubbler to incorporate water vapor, which then flows through the tube and out through the second bubbler. The second bubbler is used as a check-valve to prevent backstreaming.

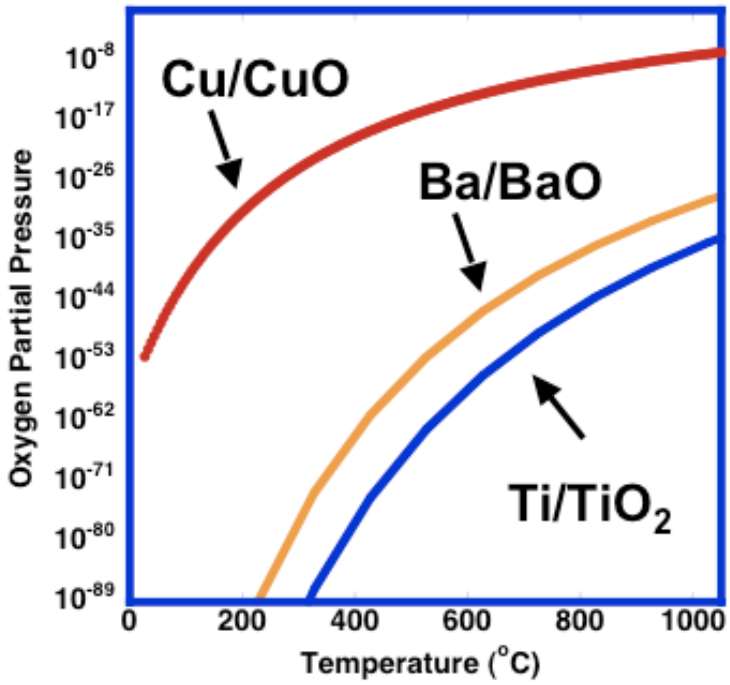

Figure 2.5: A diagram showing the equilibrium partial pressures of the metals and their oxides for the barium titanate on copper foil system.

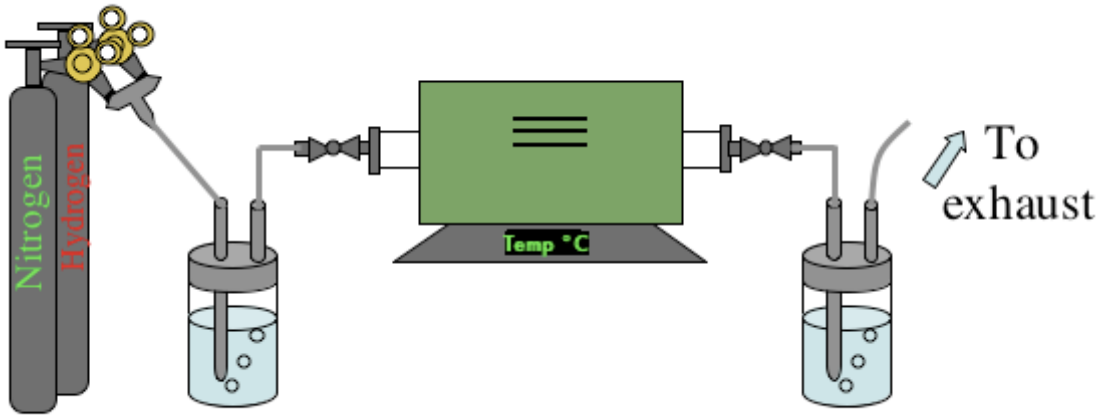

Figure 2.6: A schematic of the furnace used in these experiments. A mixture of gases is flown through a bubbler into the furnace and out through another bubbler

The process gas mixture used is comprised of N_2, H_2, H_2O and contaminant amounts of O_2. 400 sccm of N_2, which contains 1 ppm of oxygen impurity, is mixed with 20 sccm of forming gas. The forming gas is N_2 mixed with 1 mol% of H_2. The mixture is then flowed through the first bubbler where it picks up a small amount of water vapor. This mixture of gases produces an oxygen partial pressure, that is governed by the reaction in Equation 2.1. The equilibrium partial pressure for this mixture at 900 °C is 10^{-12} atm which is several orders of magnitude below that required to prevent copper oxidation.

$$H_2 + \frac{1}{2}O_2 \leftrightarrow H_2O \qquad \text{Equation (2.1)}$$

The oxygen partial pressure is measured *in situ* by an Australian Oxytrol Systems DS-Series solid-state pO_2 sensor that is located in the furnace hot zone. The oxygen sensor generates a voltage signal that is created by comparing the oxygen concentration gradient between the hot zone and the normal atmosphere outside the furnace. The sensor also contains a thermocouple that measures the exact temperature where the pO_2 is being measured. The oxygen partial pressure can then be calculated by Equation 2.2 where T is the absolute temperature measured by the thermocouple, E is the voltage from the sensor and the 0.209 represents the oxygen partial pressure in a normal atmosphere.

$$pO_2 = 0.209\left(\frac{-46.42 \times E}{T}\right) \qquad \text{Equation (2.2)}$$

2.5 Capacitor Formation

Thin film capacitor structures were formed by sputter deposition of Pt and/or Cu top electrodes on the crystallized BT and BST surfaces. This is done by sputtering a thin film of platinum or copper through a shadow mask that is placed on top of the film. Electrodes were deposited using a 2-inch DC magnetron sputtering gun with a power of 75 watts in argon gas at a pressure of 30 mTorr. The standard shadow mask contained five different circular electrode sizes ranging from $6x10^{-4}$ to $2x10^{-3}$ cm^2. A complete overview of the capacitor formation process can be seen in figure 2.7.

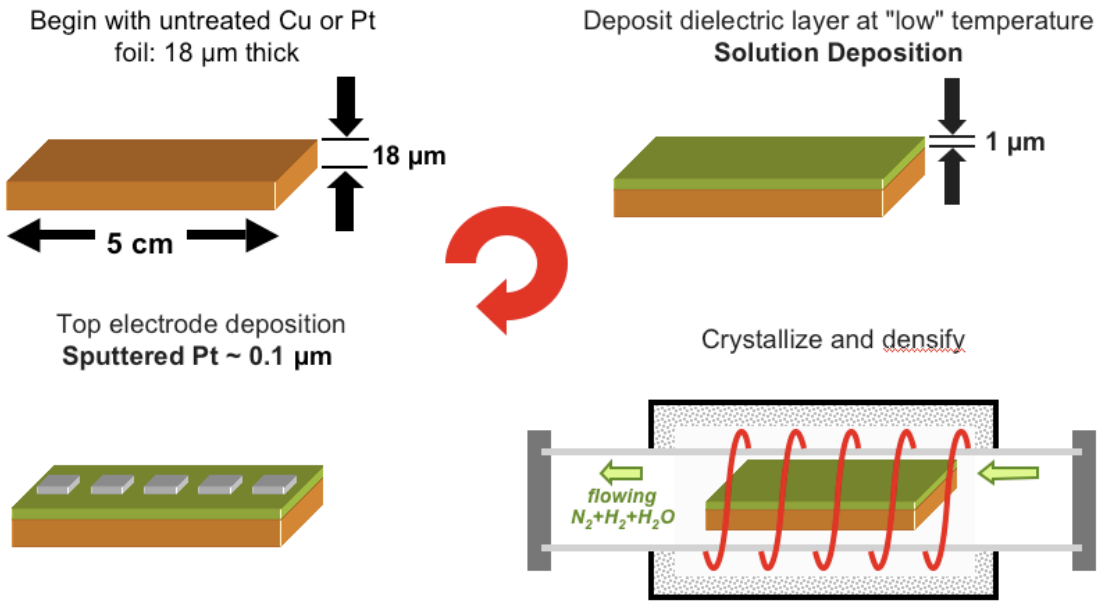

Figure 2.7: An overview of the capacitor forming process. Starting with an untreated substrate which is coated with dielectric, annealed, and finally electrodes are deposited to complete the thin film capacitor.

The primary electrical measurements were capacitance vs. voltage and capacitance vs. frequency and were carried out using an HP 4192A impedance analyzer. This machine allowed for the determination of loss tangent, permittivity and the dielectric tunability characteristic of ferroelectric materials. The frequency and voltage dependencies give valuable insight into the mechanisms of high permittivity and leakage. Measurements were taken with an oscillator voltage of 0.05 volts.

Capacitance versus temperature measurements were also collected to identify and characterize the ferroelectric phase transitions. These measurements were performed using the impedance analyzer in conjunction with an MMR Technologies

cryogenic temperature stage (model R2105). Samples were heated to 550 K and measurements of capacitance were taken as the sample was cooled to 100 K. Electrical measurements are only performed after a capacitor is determined to be functional. A functional capacitor is defined as having a loss tangent less than 0.15 with an oscillator voltage of 0.05 V at a frequency of 10 kHz under 0 bias.

The following series of figures show temperature, voltage, and frequency dependent plots of permittivity for both sputtered BST and stoichiometric BT thin films. These data represent the dielectric properties that are routinely observed and serve as a baseline for reference and comparison for this work and other literature reports.

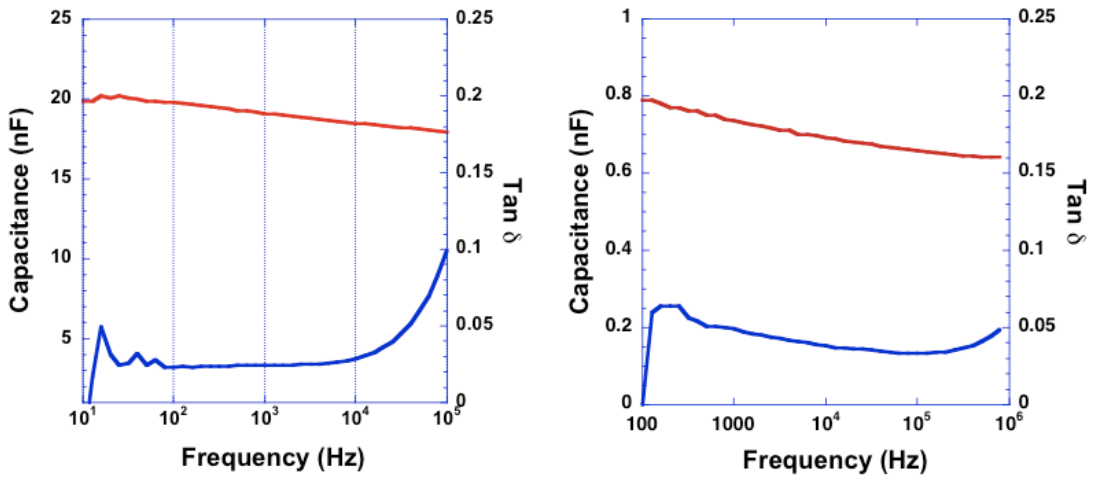

Figure 2.8: Typical electrical characterization of capacitance measured as a function of frequency for a sol-gel prepared sample on a copper foil substrate (left) and a sputtered film on a copper foil substrate (right).

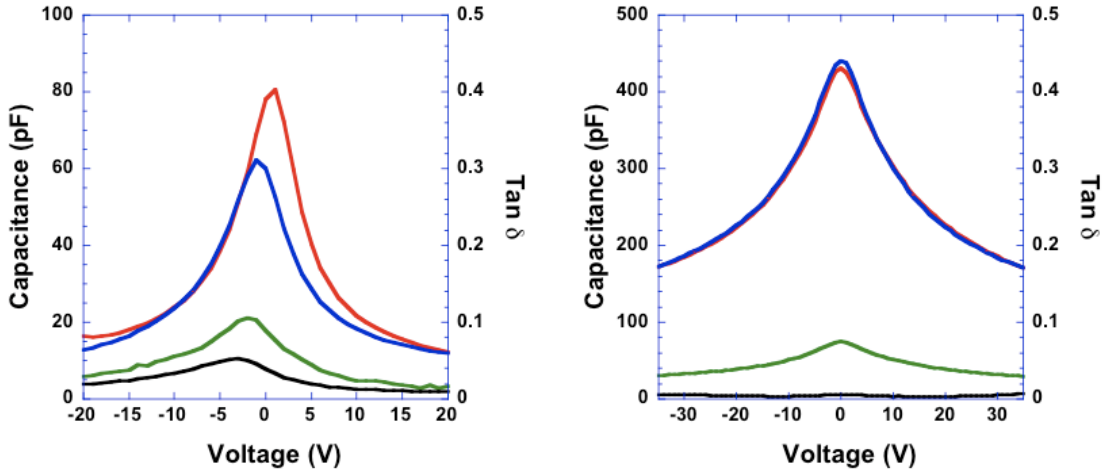

Figure 2.9: Typical electrical characterization of capacitance measured as a function of voltage for a sol-gel prepared sample on a copper foil substrate (left) and a sputtered film on a copper foil substrate (right).

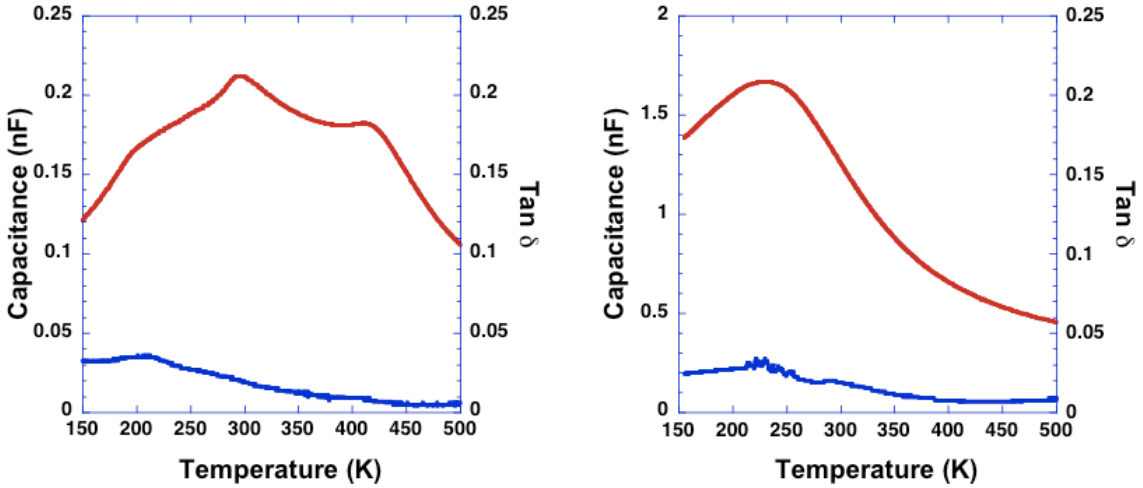

Figure 2.10: Typical electrical characterization of capacitance measured as a function of temperature for a sol-gel prepared sample on a copper foil substrate (left) and a sputtered film on a copper foil substrate (right).

2.6 Physical Characterization Techniques

The microstructure and phase assemblage of the dielectric was examined using a combination of x-ray diffraction, scanning electron microscopy and atomic force microscopy.

A Bruker AXS D-5000 x-ray diffractometer equipped with a Hi-Star area detector with a focusing circle of 15 cm was used to characterize crystal structure and phase. The focusing circle can collect approximately 35° in 2θ for any given ω setting. With proper operation and sufficient collection times, this instrument can resolve 5 nm thick films. The samples are adhered to a piece of amorphous glass by double sided tape. The piece of glass is then adhered to an aluminum stage by another piece of double-sided tape. The amorphous glass is used to separate the sample from the stage and avoid collecting diffraction information of the aluminum stage. The x-ray source and x-ray detector can be independently rotated about θ and 2θ respectively. The angles chosen for the source and detector are 15° and 30°. These angles were chosen because the 100% intensity (110) peak occurs at 31.2° in 2θ according to X-ray PDF card #34-129.

A Hitachi S-5500 Ultra-high Resolution SEM in secondary electron mode was used for examination of the microstructure. With a beam current of 10 μAmps and an accelerator voltage of 5 kV, a spot size sufficiently small was produced that could resolve 25 nm features.

A Nanosurf Easyscan 2 atomic force microscope was employed in dynamic force mode to characterize film topography. The images produced were of sufficient resolution to make an accurate determination of grain size. While the SEM provided much higher resolution, the AFM was a much faster and provided rapid feedback for process monitoring.

Using images collected via AFM and SEM, grain sizes were calculated using the linear intercept method. In this method a line is drawn in a random direction across a micrograph and the length of this line is determined by comparing the line to the micron bar using a program called ImageJ©. The intersections of the line with the grain boundaries are as follows: 1.) if the line passes through a grain boundary it is counted as 1. 2.) if the line passes through a triple point it is counted as 1/2. 3.) if a line ends within a grain it is counted as 1/2. Using this evaluation method a line is determined to be inadequate if it has a value of less than 15. If the line has a value of 15 or greater, the length of the line is divided by the line's value to determine the average grain size. This procedure is then repeated four more times on each micrograph and each value is averaged for a statistically valid grain size.

2.7 Co-firing

A portion of the experimental work utilizes a thin film co-firing process which is a derivation of the normal process flow for the production of thin films of BST and

BT on copper foils. In the co-firing process the dielectric layers are sputtered or spin coated on to the foil surface in the same fashion, but electrodes are applied prior to the annealing step. The electrode deposition technique is also different for the co-firing process. Due to the large increase in the area of the top electrode enabled by cofiring, a type of lift off technique was developed to pattern the electrodes at any size within the confines of the coated foil region. The technique was developed to decrease the amount of handling that had to be done with the sample. In the conventional process, the sample is removed from its mount used during sputtering and then fixed between a shadow mask and a backing plate using machine screws. However, this technique does not require the sample to be removed from the bracket.

Using a felt tipped marker, the area of the sample where the electrode metal is not desired is covered with an alcohol soluble ink – *i.e.*, a black Sharpie® marker. Then the sample is completely covered with the electrode metal using the previously mentioned DC sputtering technique. The electrode metal is then removed from the area of the film covered in ink by dissolving the ink with acetone. The sample is brushed lightly with a Q-tip© where the ink was placed to aid the alcohol in dissolving the ink.

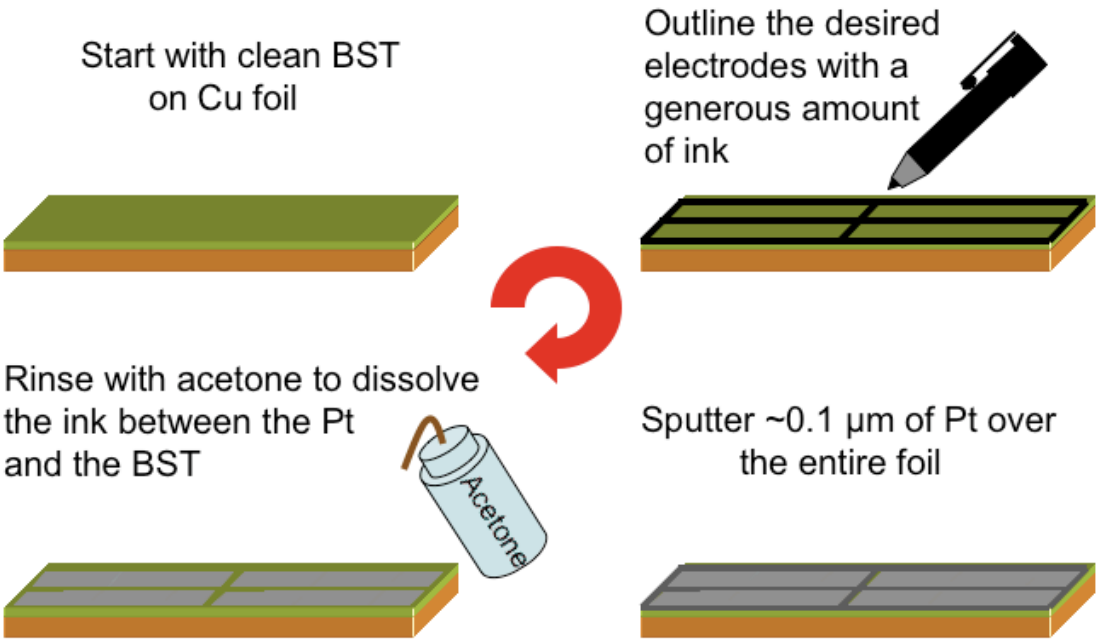

Figure 2.11: A diagram showing the lift off technique employed to produce large area electrodes and decrease handling of the thin films

Chapter 3

Chapter 3 corresponds to a manuscript that was published as a rapid communication in the Journal of Materials Research: Volume 22, Issue 7, 1763-1766, July 2007. This article was also featured as a research highlight in the November 2007 Materials Research Bulletin

Smart Electrodes for Ultra-Large Area Thin Film Capacitors

Patrick Daniels, Jon Ihlefeld, and Jon-Paul Maria
North Carolina State University
Department of Materials Science and Engineering
Campus Box 7919 Raleigh, NC 27606

William Borland
Dupont Electronic Technologies
14 T.W. Alexander Drive, P.O. Box 13999, Research Triangle Park, NC 27709

contact author information
jpmaria@ncsu.edu
phone: (919) 513-2843
fax: (919) 515-3419

Keywords: ferroelectric, film, capacitor, $BaTiO_3$, electrode

A "smart" process suitable for preparing metal-insulator-metal thin film capacitors with sub-micron insulating layers and cm-scale lateral dimensions is presented. This provides a revolutionary advance in oxide thin film applicability in implementations where semiconductor process flows are cost-prohibitive. The technique provides a 4 order of magnitude improvement in device yield and does not require sophisticated deposition equipment or a clean room environment. The key to improved yield is choosing a metal and oxide combination where the metal-oxide surface energy is greater than the metal-vapor surface energy. If satisfied, partial electrode dewetting during the high temperature anneal naturally coerces electrode metal away from geometric asperities with high curvature. Through-the-film-thickness defects that compromise layer integrity are thereby naturally avoided. This methodology is not material specific, and only requires a top electrode with a large contact angle to the dielectric in question. These are referred to as "smart electrodes" given their natural propensity to avoid film flaws.

All BST films prepared for this study were deposited by RF magnetron sputtering from a ceramic target of composition $Ba_{0.8}Sr_{0.2}TiO_3$. In all cases 18 μm thick copper foil substrates were used. Films were deposited at a substrate temperature of 100 °C for 120 minutes yielding a dielectric thickness of 800 nm. Following deposition, the films were tube-furnace annealed at 900 °C in a flowing atmosphere of 400 sccm N_2 (from a liquid dewar) and 20 sccm forming gas ($1\%H_2$:$99\%N_2$) which yields an oxygen partial pressure of 10^{-12} atm. For the conventional process shadow

masks defined sputtered Pt dots to complete the capacitors after annealing. A full description of this process is available in the literature[30]. Figure 3.1 shows the yield, or percent functional capacitors as a function of capacitor diameter. Functionality is defined as a dielectric loss tangent of less than 0.15 at 2 V dc bias. These yield percentages are well below the levels necessary for commercialization and mass production[31,32].

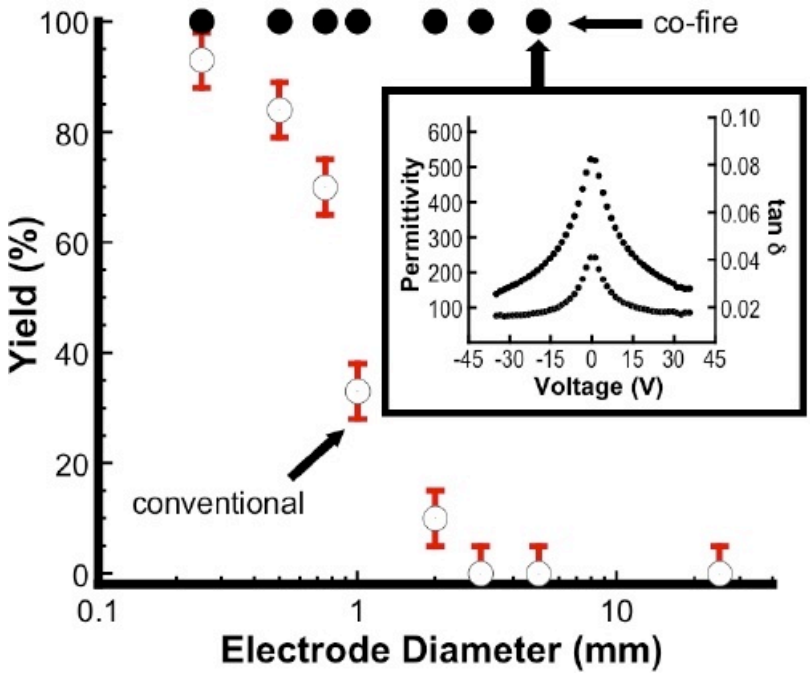

Figure 3.1: Yield as a function of electrode diameter for Pt – BST – Cu metal insulator metal capacitors. The open circles represent conventionally processed material, while the closed circles represent co-fired devices. In this case we define yield as the percent functional capacitors where functional is defined as a capacitor with tan d<0.15 at 2 V applied. The inset corresponds to a permittivity versus voltage curve for a co-fired BST capacitor with a 5 mm electrode diameter.

Defects that compromise film integrity are common, and for oxides, the most important may be categorized as follows: (1) pinhole formation during deposition, (2) crack formation from differential densification, (3) cracking promoted by residual thermal expansion mismatch strain, and (4) particle contamination. Differential densification stems from as-deposited non-uniformity caused by shadowing effects, or local substrate undulation, *i.e.*, the side of a hillock or substrate scratch. Upon heat treatment, these non-uniformities can densify at locally variable rates and result in crack formation. Thermal expansion coefficient mismatch can establish residual film stress upon heating or cooling and lead to film cracking or buckling, while particulate contamination can lead to shadowing and chemical reaction upon firing. Our SEM analyses of numerous BST films confirm the presence of these mechanisms, with differential densification being the most frequently observed.

Since the probability of depositing an electrode over such a defect scales with capacitor dimension, limitations in yield can be traced to defect area density. To ameliorate this condition, two approaches can be adopted: 1) defects are eliminated, or 2) defects are tolerated. Ultra-smooth substrates, dielectrics, and top metallization layers can be prepared in clean conditions, and deposition methods can be optimized to dramatically reduce particulates and maximize film homogeneity. Such methods have enabled dramatic success in the semiconductor industry, however, for comparatively low-cost applications like embedded passives similar measures are not suitable.

Consequently, we have developed a process by which the poor metal-oxide wetting is used to recognize and avoid film defects.

It is well known that the work of adhesion values between many electrode metals and oxide surfaces are small. Consequently, contact angles are large, and at elevated temperatures there is a propensity for dewetting[33-35]. As such, a driving force exists that can be used to move top electrode material after deposition. Even though the heat treatment temperatures used in this study are well below the melting temperature of Pt, the mass transport at 900 °C is sufficient to dramatically rearrange thin Pt films. Figure 3.2 shows two SEM images of Pt deposited on a BST surface after a 900 °C firing schedule for 30 minutes.

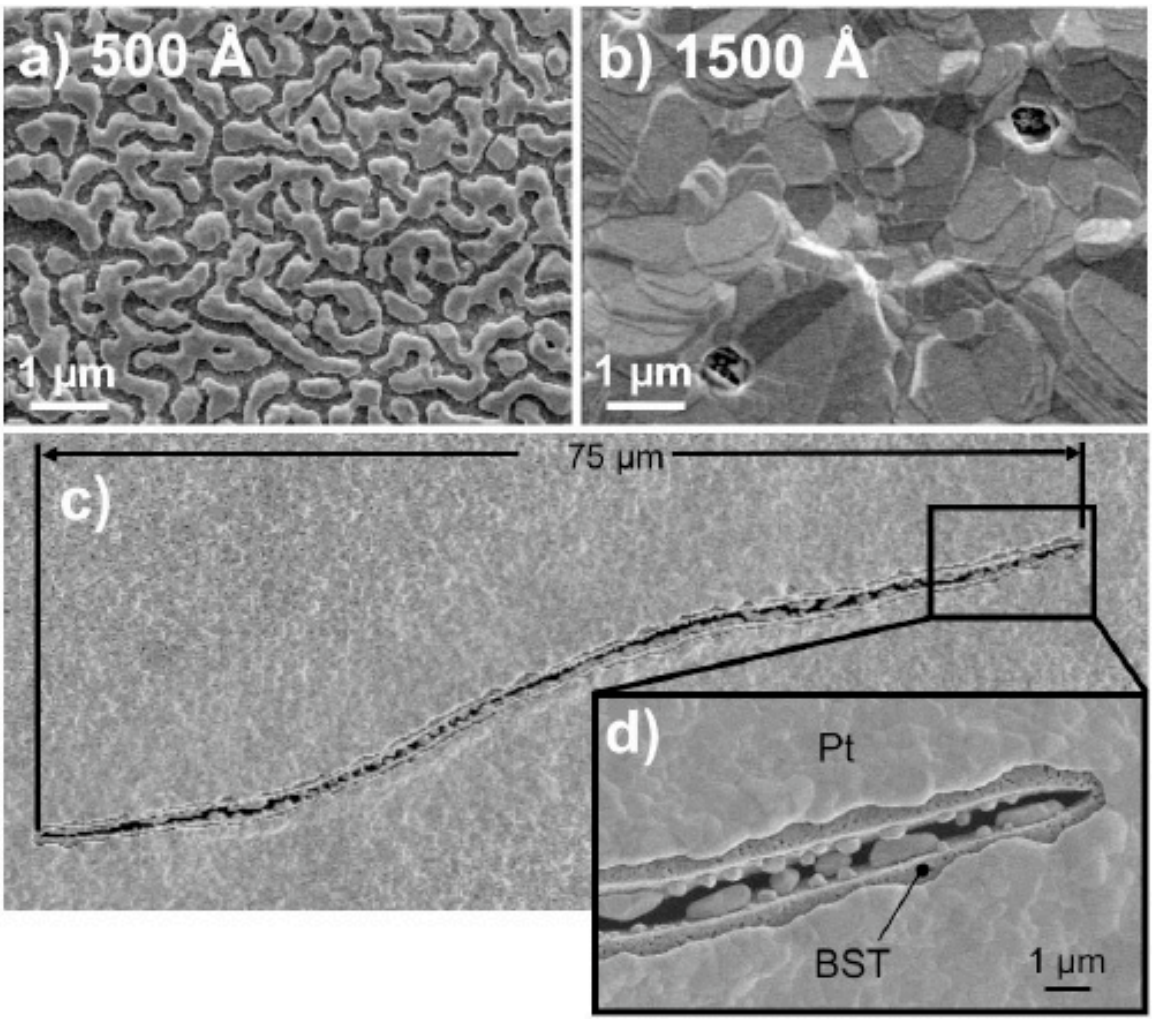

Figure 3.2: a) SEM image of a 50 nm thick Pt top electrode after the co-firing process, b) SEM image a 150 nm thick Pt top electrode after the co-firing process, c) SEM image of a large crack in an electrically functional BST capacitor, and d) A higher magnification SEM image showing that the top electrode retreats from the crack edge thereby avoiding a short circuit.

In panel (a) the Pt as-deposited thickness is 50 nm, while in (b) the as-deposited thickness was 150 nm. These images identify two important findings: at 900 °C Pt is very mobile and can rearrange to minimize BST-PT contact area, and a critical Pt

thickness exists above which dramatic rearrangement can be arrested. An electrode thickness study was conducted using 25 nm thickness intervals between 50 and 150 nm.SEM analysis of this series showed that 150 nm was required to avoid full de-wetting. Ideally, partial de-wetting around cracks is desired, while full de-wetting to a discontinuous electrode is not. We hypothesize that this behavior can be exploited to improve capacitor yield via the mechanism proposed and illustrated in figure 3.3.

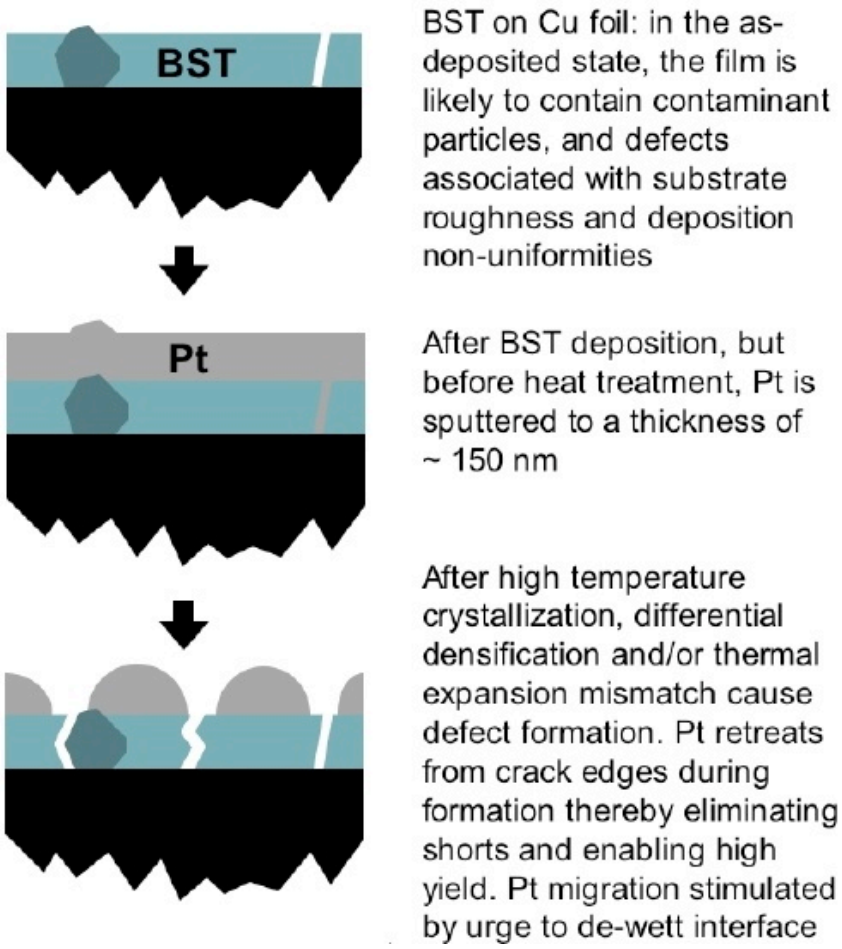

Figure 3.3: Illustration of the proposed mechanism for high yield in co-fired metal-insulator-metal BST capacitors.

At high temperatures, when the electrode material can self-diffuse to minimize interfacial energy it will preferentially avoid film defects (like film cracks) since these locations exhibit large curvature thus require a larger metal-oxide contact area per Pt volume. If BST films are metallized prior to annealing, upon heat treatment the top metal will redistribute away from high curvature defects that were present in the as-deposited state or that formed upon heating. If this redistribution occurs the yield should improve dramatically as compared to capacitors prepared via a conventional process. As an initial test, BST capacitors with a range of electrode diameters were prepared using the co-firing concept with 150 nm of sputtered Pt (using a shadow mask) before the crystallization/densification anneal. Data are shown in figure 3.1 where 100% yield was observed for electrode diameters up to 5 mm. The inset in figure 3.1 shows C-V data for a 5 mm diameter capacitor, this voltage tolerance was observed routinely in capacitors with mm-scale electrodes.

To test this hypothesis directly, films were prepared with intentional cracks that could be found and monitored by SEM. To prepare cracked thin film samples, pure barium titanate films were prepared on copper foils by chemical solution deposition following our group's well-established route[36]. To ensure cracking, an incomplete drying step was used which results in large crack formation of the pre-fired film - this is a common problem for chemical solution deposition, especially for high molarity solutions, and is linked to solvent extraction after gel consolidation[37]. Pt top electrodes

were applied by magnetron sputtering, and the identical firing procedure was performed. Post firing SEM images show the existence of these drying cracks. Figure 3.3 shows one of these cracks after the firing process, the lower magnification panel spans the entire crack, while the inset magnifies one end. Inspection of this image shows that Pt does not bridge the insulating layer at any point. Images were taken for the entire crack, and Pt was found to retreat from the edge along the entire periphery. Most importantly, this crack occurred near the center of a 2 mm diameter top electrode of a functional capacitor.

Once this mechanism was observed and identified, experiments were conducted to explore the limits of capacitor yield. A shadow mask was prepared with 25 mm x 25 mm openings. Four capacitors could be fabricated in one BST deposition, as limited by the 4" diameter BST sputter target, and were electroded and fired identically to the previous devices. The results of dielectric testing are shown in figure 3.4 where low loss tangents and permittivity values typical of sputtered BST are observed. Note that the increase in loss tangent above 100 Hz is due to the approach of resonance for this 5 μF capacitor. We note that these large capacitors did not have the voltage tolerance of the smaller sizes, however, 10 V could be applied without breakdown. After ten 25 mm x 25 mm fabrication runs, a success rate of 85% was determined.

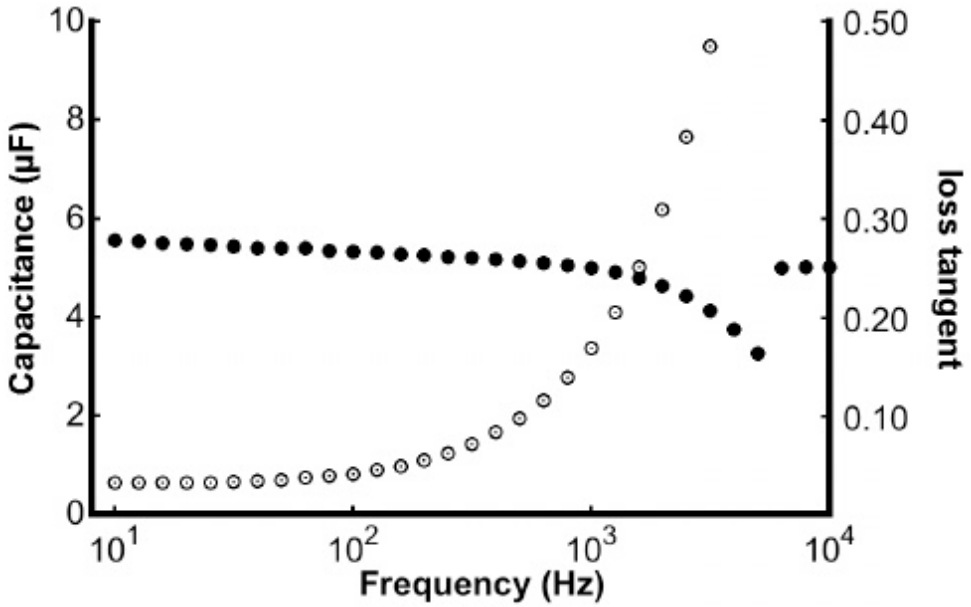

Figure 3.4: Capacitance versus measurement frequency trace for a 2.5 cm x 2.5 cm capacitor. Note that the frequency response is flat until approximately 1 kHz at which point resonance is approached. This low frequency resonance is a consequence of impedance matching to a 5 μF capacitor, not a material response.

In summary, a co-firing process that enables a 10^4 improvement in capacitor yield is presented. Using this process, parallel plate capacitors with aspect ratios of 10^4 were prepared and single layer thin film devices with capacitance values of 5 μF were demonstrated. This process requires no specialized deposition equipment or clean room environment. The success of this process results from the large surface energy between many oxide dielectrics and many transition and noble metals. This interfacial characteristic is believed to drive material redistribution at high temperatures. Most importantly, the redistribution directs material away from regions of large curvature, like crack edges and pinholes. Direct evidence of this mechanism was found by scanning electron microscopy. This method can be used to routinely prepare square

parallel plate capacitors with one micron thick insulating layers and 25 mm edge lengths.

References

1. B. Laughlin, J. Ihlefeld, and J. P. Maria, "Preparation of sputtered $(Ba_{1-x},Sr_x)TiO_3$ thin films directly on copper." *J. Amer. Ceram. Soc.,* **88[9]**, 2652-2654 (2005).

2. T. Horikawaet al. "Dielectric properties of $(Ba,Sr)TiO_3$ thin-films deposited by RF-sputtering." *Jap. J. Appl. Phys. Part 1-Regular Papers Short Notes & Review Papers* **32[9B]**, 4126-4130 (1993).

3. N. K. Pervez, P. J. Hansen, and R. A. York, "High tunability barium strontium titanate thin films for rf circuit applications." *Appl. Phys. Lett.* **85[19]**, 4451-4453 (2004).

4. D. P. Cann, *Thermochemical interactions at electrode interfaces in electroceramic applications*. Ph.D. Thesis, The Pennsylvania State University, (1997).

5. D. Chatain and C. Carter, Wetting dynamics - Spreading of metallic drops." *Nature Materials*, **3**, 843-845 **(2004)**.

6. M. McLean and E. D. Hondros, "Study of grain-boundary grooving at platinum/alumina interface." *J. Mat. Sci.* **6**, 19-23 **(1971)**.

7. J. Ihlefeld, B. Laughlin, A. Hunt-Lowery, W. Borland, A. Kingon, and J-P. Maria, "Copper compatible barium titanate thin films for embedded passives." *J. Electroceramics*, **14[2]**, 95-102 (2005).

8. R. W. Schwartz, T. Schneller, and R. Waser, "Chemical solution deposition of electronic oxide films." *Chimie*, **7**, 433-461 (2004).

Chapter 4

Chapter 4 corresponds to a manuscript that was submitted to the Journal of Materials on May 29, 2007. The manuscript is currently under review.

Property engineering in $BaTiO_3$ films by stoichiometry control

P. R. Daniels, S. M. Aygün, and J-P. Maria
Department of Materials Science and Engineering,
North Carolina State University
Raleigh, NC 27606 USA

J. F. Ihlefeld
Department of Materials Science and Engineering,
Pennsylvania State University
University Park, PA 16802 USA

W. Borland
Dupont Electronic Technologies,
Research Triangle Park, NC 27709 USA

4.1 Abstract

$BaTiO_3$ thin films were prepared on metallic foil substrates using chemical solution deposition. The impact of *A*-site to *B*-site cation ratios was investigated by characterizing a sample set that includes stoichiometric $BaTiO_3$ and 1, 2, 3, 4 and 5 mole percent excess barium oxide. Each composition was subjected to a high temperature anneal step with maximum dwell temperatures of 1000, 1100 and 1200 °C for 20 hours. Excess barium concentrations greater than 3% lead to dramatic grain growth and average grain sizes exceeding 1 μm. Despite the large deviations from stoichiometry and the 20 hour dwell time at temperature, x-ray diffraction and high-resolution SEM analysis were unable to detect second phases until films with 5% excess barium were annealed to 1200 °C. Thin films with 3% excess barium were prepared on Cu substrates and annealed at 1060°C – the practical limit for Cu. This combination of BaO excess and annealing temperature produced an average lateral grain size of 0.8 microns and a room temperature permittivity of 4000. This is in comparison to a permittivity of 1800 for stoichiometric material prepared using identical conditions. This work suggests metastable solubility of BaO in $BaTiO_3$ which leads to enhanced grain growth and very large permittivity values. This technique provides a new solid-state means of achieving grain growth in low thermal budget systems.

4.2 Introduction

A film-based capacitor technology suitable for lamination into integrated circuit boards is highly desired in the electronics packaging industry. Such a technology would require high capacitance density, suitable breakdown voltage, and low production cost.[38-40] Since the late 1990s, several groups have pursued a film-on-foil approach where high permittivity dielectric layers are synthesized on thin metal foils and subsequently laminated into printed wiring board panels.[4,25,41,42] More recently, a smart electrode process has been developed that allows large area electrodes to be formed on foil substrates with substantial roughness[43]. Though these processes have overcome several of the technology challenges and are consistent with physical integration and general low cost, a substantial increase in capacitance density is still required. In most cases, the technology is limited to ~ 2 $\mu F/cm^2$ and high value added applications demand $\geq 5\ \mu F/cm^2$.[38]

Two methods are available to increase the capacitance density of $BaTiO_3$ thin film capacitors in the metal-insulator-metal configuration. One is to decrease the physical thickness of the dielectric layer, however, with film thickness typically less than 1 micron, a meaningful decrease in the dielectric thickness would compromise reliability since film thickness would become comparable to foil roughness. The second method is to increase the permittivity of the dielectric layer which is usually smaller than that observed in bulk crystals. In order to increase permittivity, two conditions must be met. 1) The grain size must be engineered to levels consistent with

the 0.7 μm maxima observed in ceramic systems;[44] and 2) processing steps that increase crystal quality of the individual $BaTiO_3$ grains must be incorporated.[13,45] Frey and Payne demonstrated that ceramic barium titanate can be prepared with 300 nm grains and room temperature permittivity values in excess of 4000.[6,10] Consequently, it is only the limitations of processing science that regulate ultimate thin film capacitor performance.

Previous investigations have shown that incorporating liquid phases in $BaTiO_3$ films can lead to large grains, high crystalline quality, and permittivity values equivalent to bulk ceramic counterparts[41]. However, in situations where substantial liquid phase is present, Ostwald ripening can become difficult to uniformly control. The same authors also showed that a modest increase in $BaTiO_3$ grain size could be achieved through the addition of excess barium at 900 °C, presumable via a defect mechanism that enhances solid-state diffusion[27]. This study expands on this previous work by exploring a wider range of compositions and temperatures. Ultimately, this report uncovers broad metastable solubility for BaO in $BaTiO_3$, illustrates the utility of this solubility for microstructure and property enhancement, and raises new questions regarding the $BaTiO_3$ phase diagram under the thin film boundary conditions.

4.3 Experimental Procedure

$BaTiO_3$ thin films were prepared using a chemical solution deposition process developed by Ihlefeld, *et al*[36]. Two solutions were prepared concurrently. One solution

involves the chelation of the transition metal alkoxide titanium(IV)-isopropoxide with acetylacetone and diethanolamine: the *B*-site solution. The other solution consists of barium acetate dissolved in acetic acid: the *A*-site solution. The solutions are then combined in amounts that will produce the desired stoichiometry with a concentration of 0.3 molar. Solution stoichiometries ranged from 0 to 5 mole percent excess barium. These solutions were then spin coated on Pt, Cu and Ni foils. Films were spun at 3000 rpm for 30 seconds and dried on a hotplate for 5 minutes at 250 °C after each deposition. The process was repeated 6 times and results in a film thickness ~700 nm after annealing. The rolled Pt, electroplated Cu, and rolled Ni foils were x μm, y μm, and z μm thick, and were supplied by vendor 1, vendor 2, and vendor 3 respectively.

For films prepared on Pt foils, the film/foil stack was fired in air at temperatures of 1000, 1100 and 1200 °C for 20 hours. Films prepared on Cu foils were annealed for 20 hours at temperatures of only 1000 and 1060 °C because of the copper melting temperature of 1084 °C. The annealing step for a film on Cu was done in a low pO_2 atmosphere consisting of 400 sccm flowing N_2 and 20 sccm 99%N_2:1%H_2 bubbled through room temperature water to establish an oxygen partial pressure that prevents the oxidation of the Cu foil at high temperatures. At the dwell temperature, pO_2 values were measured *in situ* to be 10^{-13} atm and 10^{-10} atm, at 900 °C and 1060 °C respectively.

A Bruker AXS D-5000 x-ray diffractometer was used to characterize crystal structure and phase. A Nanosurf Easyscan 2 atomic force microscope was employed in

dynamic force mode to characterize film topography. Electrical measurements were collected using an HP 4192A impedance analyzer (oscillator frequency of 10 kHz and amplitude of 50 mV) and an MMR Technologies cryogenic temperature stage (temperature dependent measurements were collected during cooling). Electrical measurements required the deposition of 50 nm thick Pt shadowmask defined electrodes by dc magnetron sputtering. SEM images were collected using a Hitachi S-5500 Ultra-high Resolution SEM in secondary electron mode.

4.4 Results and Discussion

4.4.1 Part 1- $BaTiO_3$ on Pt

After deposition and firing, atomic force microscopy (AFM) and x-ray diffraction (XRD) were performed to evaluate the surface microstructure and crystallinity. Figures 4.1, 4.2, and 4.3 show AFM micrographs of stoichiometric, 3% excess BaO, and 5% excess BaO films fired at 1000, 1100 and 1200 °C, respectively (for brevity 2% and 4% excess BaO are not shown). Inspection of these data reveals a trend of increasing grain size when increasing both temperature and Ba excess. For stoichiometric $BaTiO_3$, the increase in grain size with temperature was minimal, whereas dramatic increases in grain size were seen for samples with 3% and 5% BaO excess. The only exception to this trend occurred for samples with 5% BaO excess annealed to 1200 °C, in which case grain growth was modest. Figure 4.4 summarizes

the average grain size vs. composition and temperature as computed by linear stereology.

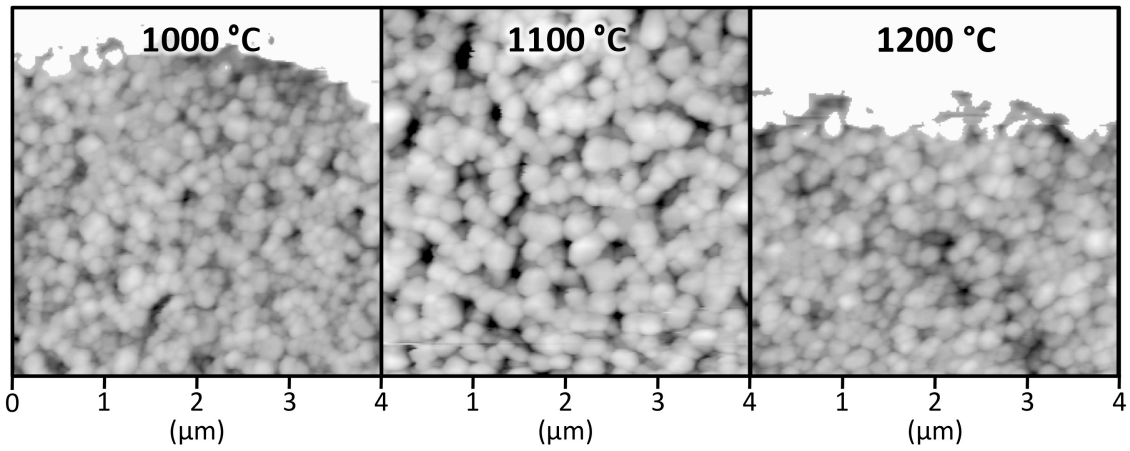

Figure 4.1: AFM images of stoichiometric $BaTiO_3$ films on Pt foils processed with a final annealing temperature of 1000 °C, 1100 °C, and 1200 °C for 20 hours respectively. Negligible grain growth is seen in this temperature range.

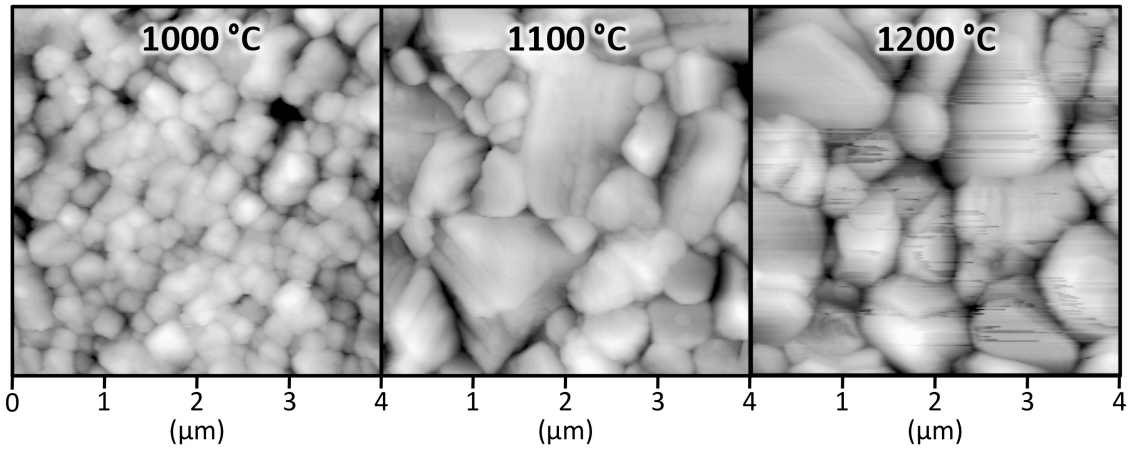

Figure 4.2: AFM images of $BaTiO_3$ films with 3% excess BaO on Pt foils processed with a final annealing temperature of 1000 °C, 1100 °C, and 1200 °C for 20 hours respectively. Substantial grain growth is seen above 1000 °C.

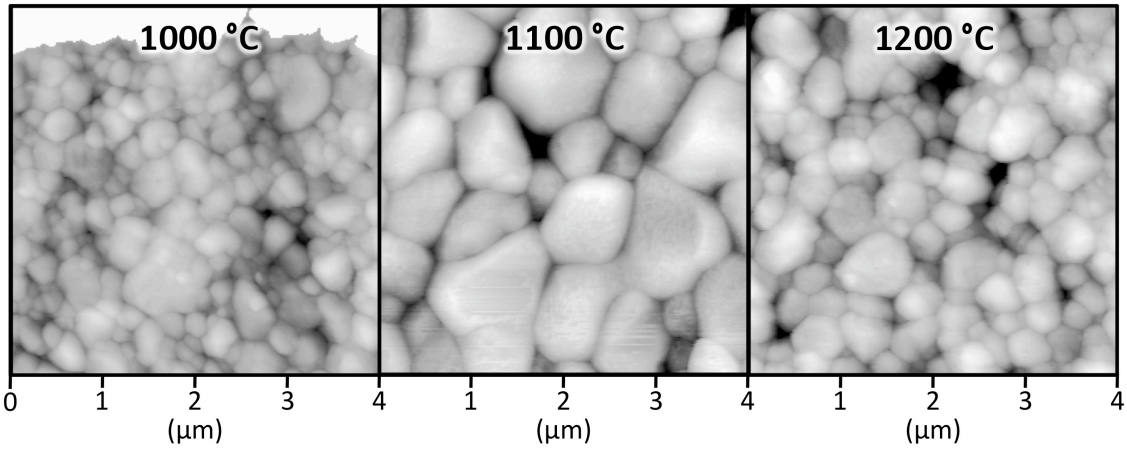

Figure 4.3: AFM images of $BaTiO_3$ films with 5% excess BaO on Pt foils processed with a final annealing temperature of 1000 °C, 1100 °C, and 1200 °C for 20 hours respectively. substantial grain growth is seen above 1000 °C, with a reduction of grain size at 1200°C.

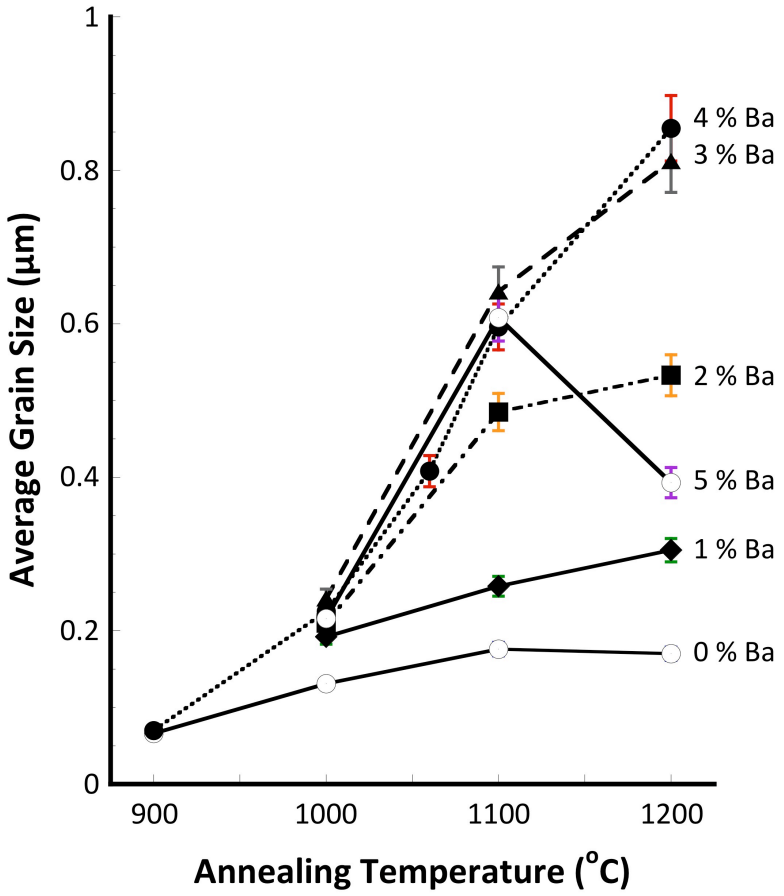

Figure 4.4: Summary of grain size as a function of annealing temperature and BaO excess. The labels on the right hand side of the figure indicate the quantity of excess BaO in each sample set.

XRD analysis for the composition series annealed to 1200 °C is shown in figure 4.5. Despite the large deviations from stoichiometry and the 20 hour heat treatments, in only one case: 1200 °C and 5 % BaO excess, could a crystalline second phase be identified by XRD. Diffraction analysis for all other temperatures indicate phase pure $BaTiO_3$. As shown in figure 4.4, this peak is consistent with the Ba_2TiO_4 orthotitanate

phase as the 100% intensity 222 reflection becomes visible. This data suggests a level of solid solubility in $BaTiO_3$ that has not been previously reported.

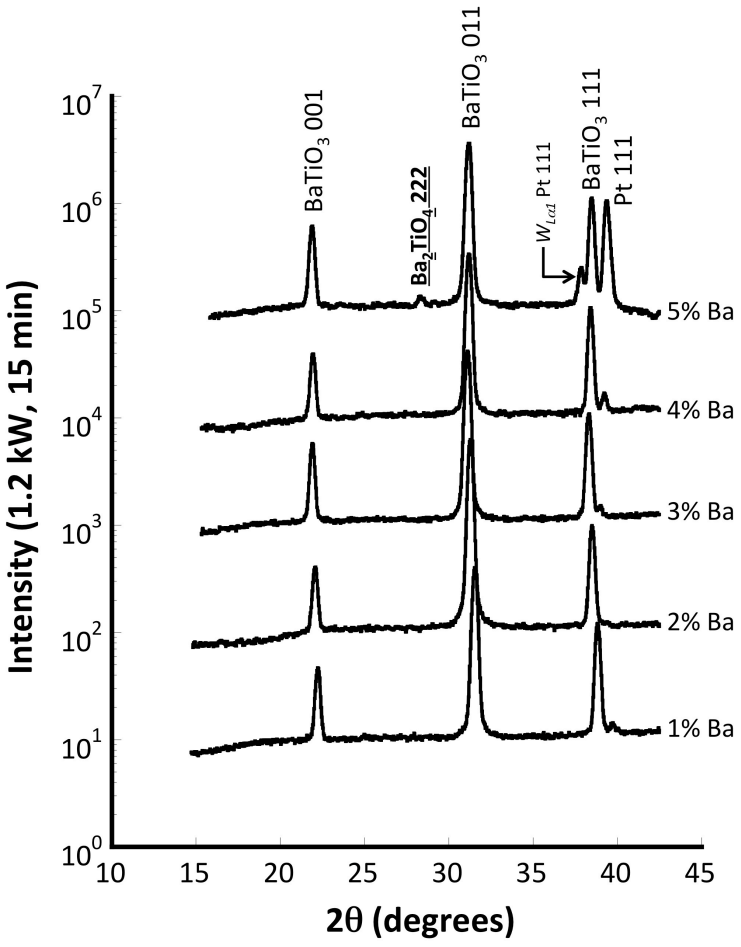

Figure 4.5: XRD analysis of $BaTiO_3$ composition series annealed at 1200 °C for 20 hours. The labels on the right hand side of the figure indicate the quantity of excess BaO in each sample. Note that temperatures higher than 1100 °C and > 4% BaO excess are required to precipitate a second crystalline phase.

Next, the temperature dependent electrical properties were measured for a sample with 3% excess Ba annealed at 1200 °C for 20 hours. The capacitance vs. temperature sweep in figure 4.6 shows three distinct features at temperatures

comparable to the three structural phase transitions in barium titanate. Though these features are not particularly sharp in comparison to bulk $BaTiO_3$, they are substantially less diffuse than commonly seen in thin film samples[26,41,46]. It is unusual that the peak permittivity does not occur at the ferroelectric-paraelectric phase transition, however, we do not attempt to explain the origins of this behavior in the current manuscript.

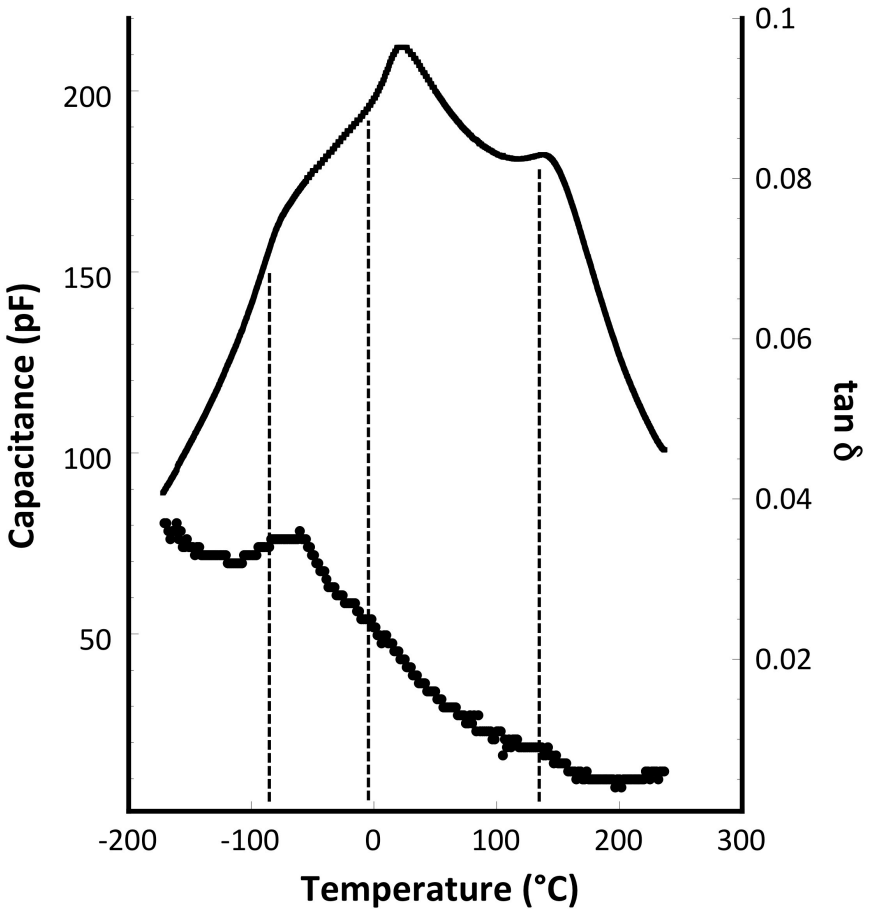

Figure 4.6: Capacitance vs. temperature measurement for a thin film of $BaTiO_3$ on platinum containing 3% excess BaO and annealed in air for 20 hours at 1200 °C. Dashed lines indicate the $BaTiO_3$ bulk phase transition temperatures.

The permittivity of the sample shown in figure 4.6 could not be calculated. This is a consequence of the extreme roughness of Pt foils. The multi-micron roughness of Pt foils and film formation by spin coating results in dielectric layers with cross sections that vary in thickness by more than a factor of two. These undulations were verified by SEM imaging and obfuscate attempts to identify a meaningful film thickness. Despite these uncertainties, the sharp temperature response and the large grain sizes suggest that permittivity values are quite large.

4.4.2 Part 2 – $BaTiO_3$ on Cu

While the Pt foils enable investigating the desired temperature range and the identification of a compositional threshold where large grain sizes can be achieved, Pt is not technologically interesting due to its high cost and incompatibility for large-scale applications. These results would be more technologically pertinent if similar properties could be produced on a commercializable substrate such as a Cu foil. Cu however melts at 1084 °C thus cannot grant access to the 1200 °C range of temperatures that produce bulk ceramic-like microstructures. However, the Pt data suggests that some degree of grain growth may be possible at the very limit of Cu stability if accompanied by a 3% BaO excess. To explore this possibility, $BaTiO_3$ films were synthesized with 3% excess BaO and annealed to 1060 °C for 20 hours. We note that at these temperatures and times, the volatility of Cu becomes problematic and to avoid substrate evaporation it is helpful to load the furnace with additional Cu blocks

or foils to minimize foil loss. Also, even slight reductions to the pO_2 lower than needed for equilibrating metallic copper with enhance the Cu evaporation rate. These films were subsequently analyzed using XRD, high-resolution scanning electron microscopy (HR-SEM) and electrical measurements.

High-resolution SEM was performed on films of stoichiometric $BaTiO_3$ and 3% excess barium $BaTiO_3$ that were annealed for 20 hours at temperatures of both 900 °C and 1060 °C. Figure 4.7 shows the microstructure comparison for the four sample types. As in the case of Pt substrates, the increase in annealing temperature did not have substantial influence on stoichiometric $BaTiO_3$ grain size, however, when annealing temperatures were raised to 1060 °C a substantial grain size increase was observed for the 3% BaO excess composition. The combination of copper foil substrates and a lower annealing temperature provided for smoother films with measureable electrode areas and uniform thickness. Dielectric measurements revealed permittivity values of 1800 and 4000 for stoichiometric and 3% excess barium thin films, respectively. The increase in grain size resulted in a doubling of the room temperature permittivity.

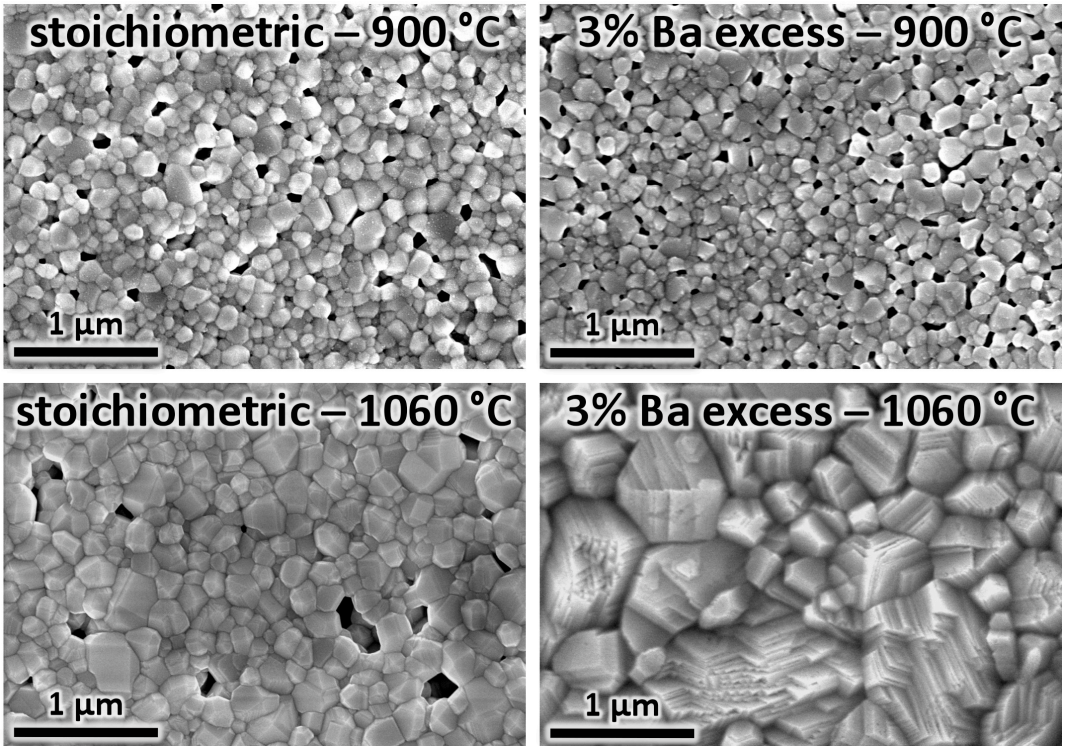

Figure 4.7: SEM micrographs of stoichiometric and 3% excess BaO films on Cu foils annealed at 900 °C and 1060 °C for 20 hours. 3% BaO excess and 1060 °C provide rapid grain growth and a copper compatible condition.

4.5 Discussion

Collectively, the data presented thus far suggest an unexpectedly broad barium solubility window – at least under these particular thin film boundary conditions. The authors hypothesize that this solubility underlies the mechanism for the observed grain growth. However, to support this hypothesis, it is necessary to do a much more rigorous search for second phases in these excess barium films. The current sample set suggests up to 4% solubility of BaO in $BaTiO_3$ even after 20 hours at 1200 °C. In comparison to previous studies, the present investigation implements a composition

further from stoichiometry, a comparable thermal budget, and x-ray diffraction analysis with in many cases greater sensitivity to the presence of small volumes of second phases. Regardless, this does not guarantee phase purity, non-crystalline materials may still be present. To investigate this possibility, we imaged the thin film surfaces, and specifically the grain boundaries using a state-of-the-art SEM with substantially higher resolution than available to many of the previous researchers (as much of the work was performed more than 20 years ago). The results of this analysis are shown in figure 4.8, again no second phases are detected in the 3% excess barium film annealed at 1200 °C. Numerous grain boundary triple points were surveyed and in all cases, the intersections contained no evidence of BaO-rich material. Figure 4.8(b) shows high magnification of several representative $BaTiO_3$ grain boundary intersections. We note that in the cases where second phases were seen by previous authors, the morphology was that of small grains at the $BaTiO_3$ boundaries. Their morphology and size would be clearly visible to the present SEM analysis. We further note that substantially more grain boundary are is covered by SEM analysis than is possible by TEM given the necessity for thin foil preparation, thus it is less likely that sparsely distributed second phases were missed.

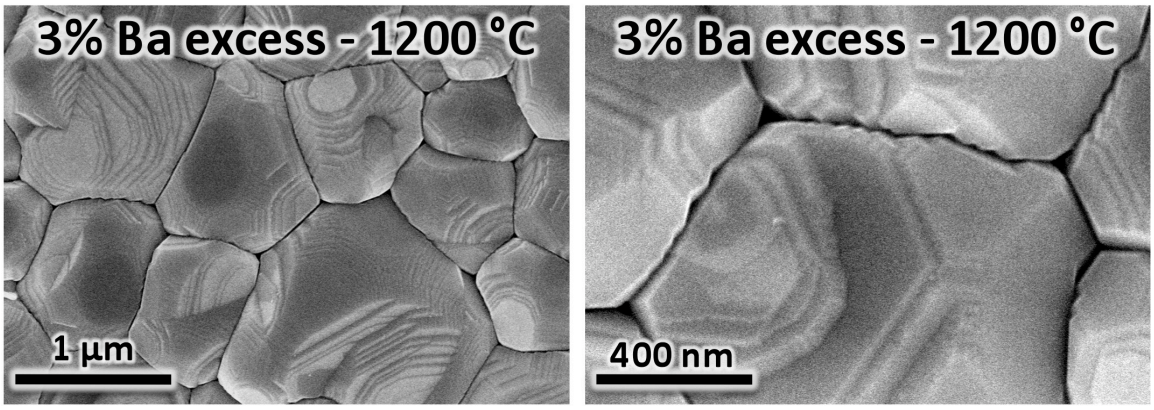

Figure 4.8: SEM micrographs of a 3% excess BaO film on platinum annealed at 1200 °C for 20 hours. The images are of the same sample and the magnifications of 35kX (left) and 120kX (right) respectively. Note that at these high magnifications, there is no evidence of second phases at the grain boundaries or the grain boundary triple points.

Controlled exposure to humidity and temperature dependent dielectric measurements were used to test the presence of BaO since in principle BaO could precipitate and the grains could be mistaken for $BaTiO_3$ in the SEM. A film of 3% excess barium on Cu annealed at 1060 °C was exposed to 100% humidity for 20 hours at 95 °C. Since barium oxide readily forms barium hydroxide in the presence of humidity,[47] if there were any BaO present, it would form $Ba(OH)_2$ and quantities that would challenge detection x-ray diffraction should produce a sharp degradation in electrical response. X-ray analysis was conducted on this sample and no hydroxide was detected after humidity exposure. Figures 4.9 and 4.10 show the temperature and frequency dependent dielectric response for the 3% excess film before and after humidity exposure with no significant changes in loss tangent or dispersion (the same dot capacitors are compared). We note that the frequency dependent data is purposely

plotted as capacitance as the absolute value is important in identifying the onset of resonance above 10^5 Hz. The small differences in these capacitors can be explained by dielectric aging during the long exposure time to temperatures close to the ferroelectric transition.

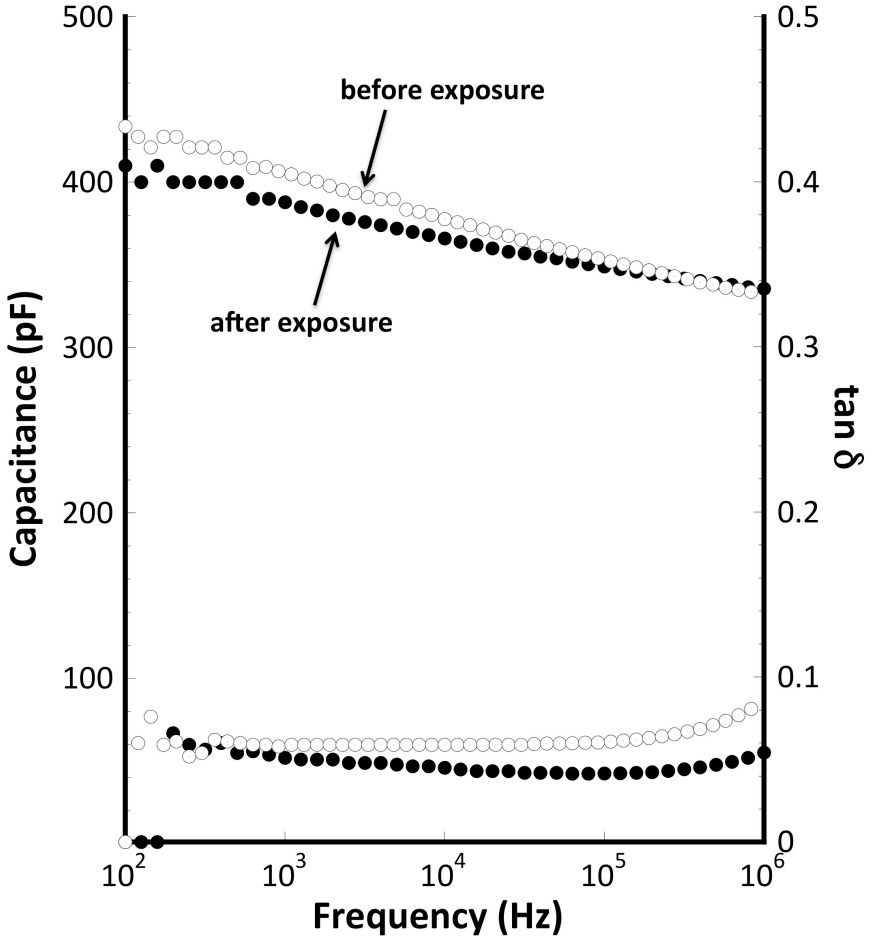

Figure 4.9: Capacitance vs. frequency measurement for a 3% excess BaO film on copper annealed at 1060 °C for 20 hours. Data are given for the as-prepared state and after exposure to 100% humidity for 24 hours.

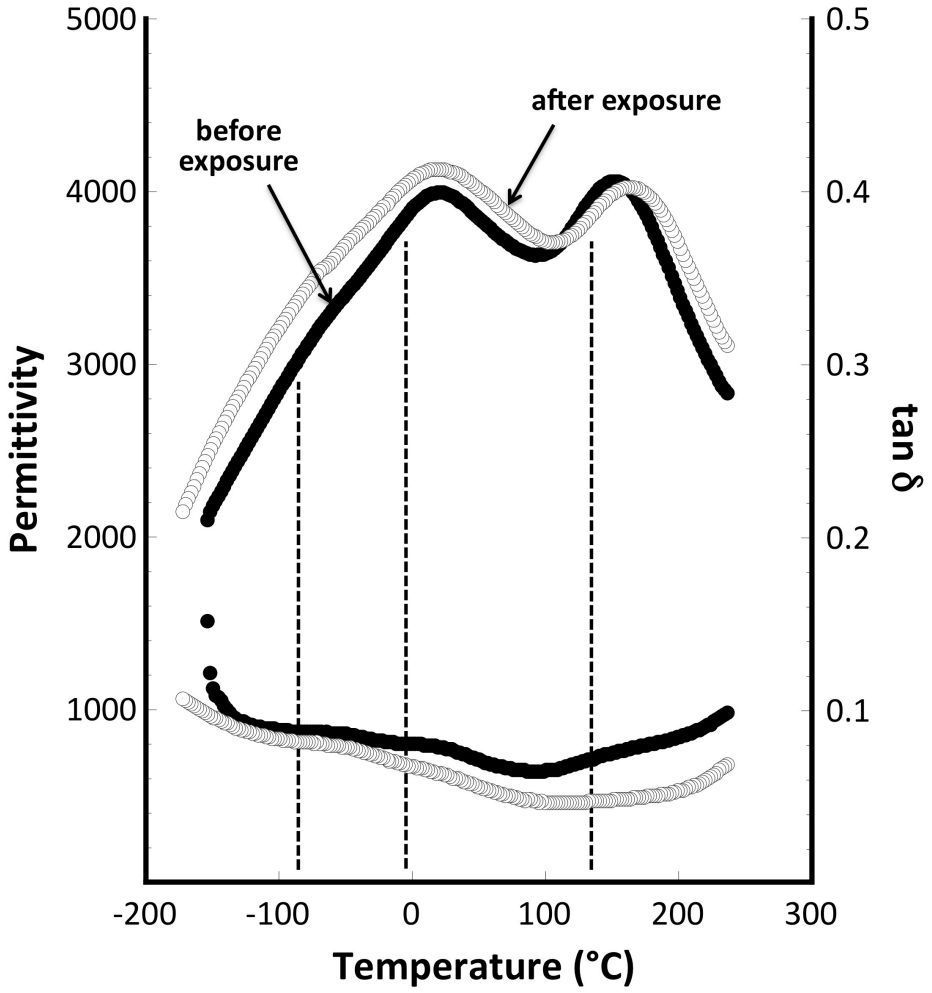

Figure 4.10: Permittivity vs. temperature measurement for a 3% excess BaO film on copper annealed at 1060 °C for 20 hours. Data are given for the as-prepared state and after exposure to 100% humidity for 24 hours. Dashed lines indicate the $BaTiO_3$ bulk phase transition temperatures.

The inability to identify second phases using diffraction, electron microscopy, or electrical analysis in the films containing substantial concentrations of excess barium suggest a level of solubility in the $BaTiO_3$ system that is substantially wider than previously observed. However, a limit to this apparent solubility can be identified.

A second phase can be seen by XRD at 5% excess barium after 20 hour annealing at 1200 °C; figure 4.11 shows an SEM image of this material. The line shaped grains are believed to be the second phase that is detected by XRD, and can be indexed as barium orthotitanate. Assuming that these bar-shaped grains extend through the film thickness with constant cross sectional area, the volume fraction of second phase is estimated to be ~5% by area mapping. Given the precursor solution stoichiometry and the densities of the $BaTiO_3$ and Ba_2TiO_4, if all excess Ba participated in orthotitanate formation, a mol fraction of ~ 4% orthotitanate in a matrix of $BaTiO_3$ would be expected. As such, we observe an abrupt, but not complete, collapse of solution stability.

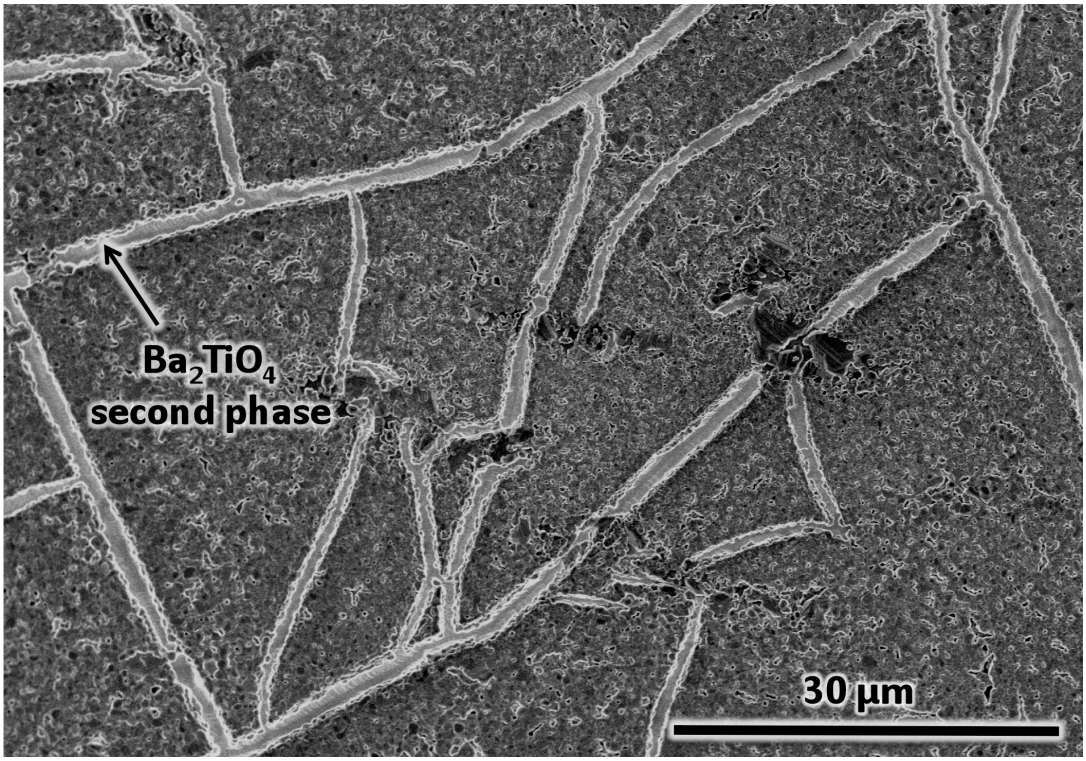

Figure 4.11: SEM image of a $BaTiO_3$ film on Pt containing 5% excess BaO annealed at 1200 °C for 20 hours. XRD measurements of this sample revealed a crystalline second phase. Area mapping of this SEM image indicates a 5% area coverage by the second phase. If the second phase is assumed to have a constant thickness equivalent to that of its matrix, it would account for ~ 4% of the entire volume.

At this point, it is important to consider the collapse of solubility and the precipitation of Ba-orthotitanate. If a true solubility window existed to ≤ 5% Ba excess, then only a very small quantity of precipitate phase would be expected. On the contrary, we observe a quantity of precipitate suggesting that nearly all excess Ba has come out of solution. Consequently, it is proposed that $BaTiO_3$ prepared in this manner can support a solubility window of up to 5% excess Ba, however, this is a metastable solution that is stabilized by extrinsic factors established by the process. Importantly,

identical solubility trends are seen for air-fired $BaTiO_3$ on Pt and for low pO_2 fired $BaTiO_3$ on Ni and Cu. This suggests that neither oxygen partial pressure nor substrate chemical reactions are responsible for the apparent solubility and grain growth.

Finally, it is important to note one addition feature regarding this data set. Despite the high firing temperatures, the long dwell times, and average grain sizes larger than 1 μm, $BaTiO_3$ films with excess Ba do not show tetragonal symmetry. Previous results for large-grained $BaTiO_3$ films on Cu by Ihlefeld *et al.*[41] demonstrated a smooth transition from pseudocubic $BaTiO_3$ to tetragonal $BaTiO_3$ when average grain size exceeded ~ 1 μm. Fig. 12 shows x-ray diffraction patterns for a film with 3% Ba excess fired to 1200 °C and a film prepared with 3% $BaO{\cdot}B_2O_3$ flux. Both films show average grain sizes ~ 1 μm but only the fluxed film shows tetragonal symmetry. From what is know regarding trends of grain size, ferroelectricity, and symmetry in $BaTiO_3$, one would fully expect tetragonal splitting in 1 μm material[10,48,49]. The authors speculate that that under these processing conditions Ba solubility is metastably achieved, and the deviation from stoichiometry result in a pseudocubic room temperature crystal structure that is similar to that observed in fine grained $BaTiO_3$. It is important to note, however, that this pseudocubic structure produces room temperature permittivity values close to 4000, which are consistent with bulk reports. This speculation raises new questions regarding the necessary crystal structures and composition ranges that promote large permittivity in $BaTiO_3$ and new possibilities for property engineering.

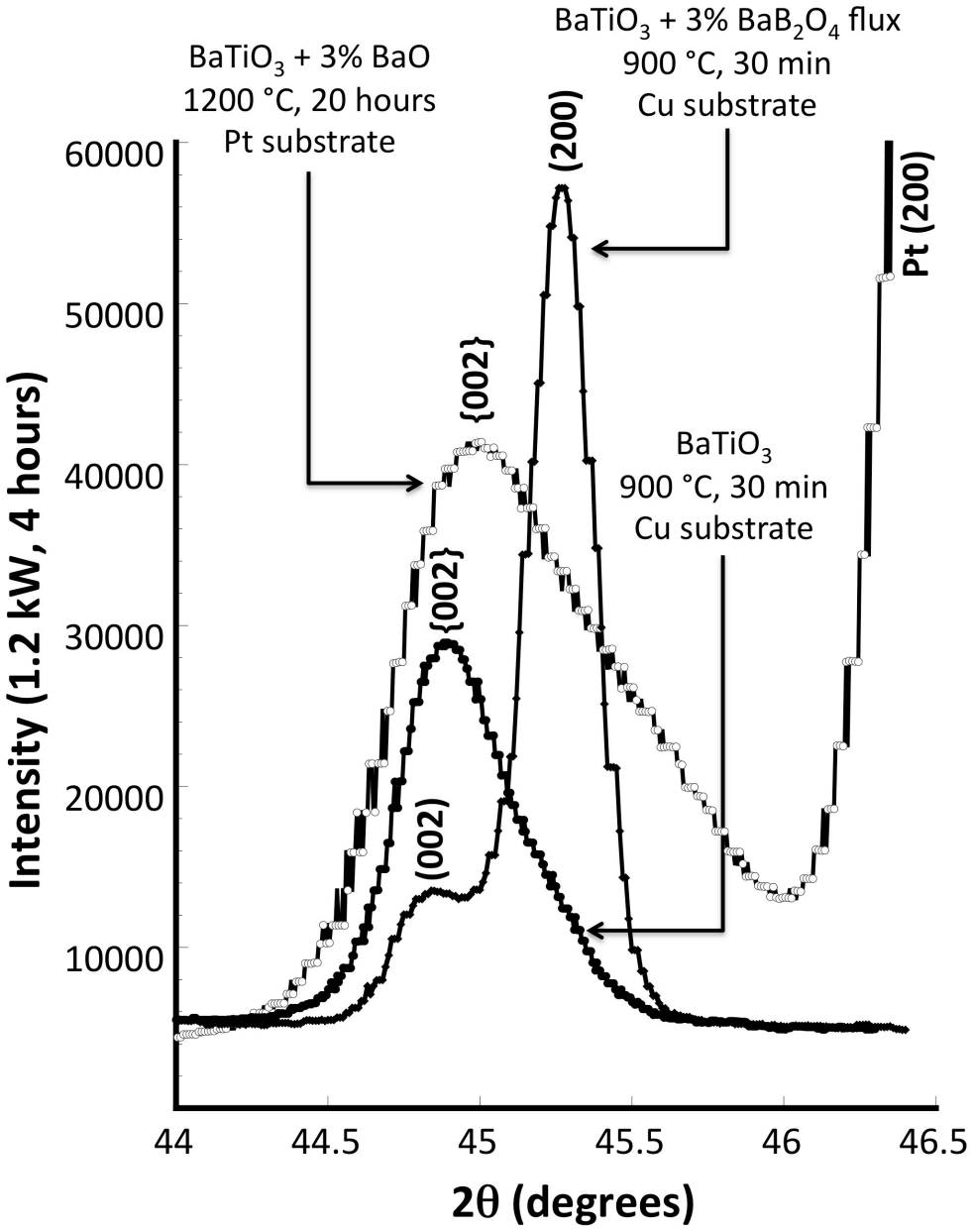

Figure 4.12: XRD patterns for the $BaTiO_3$ [25] reflection family of a stoichiometric film processed to 900 °C, a film with 3% BaO excess processed to 1200 °C, and a $BaO \cdot B_2O_3$–fluxed film processed to 900 °C (from reference 4). Note that the BaO excess and the fluxed $BaTiO_3$ both have average grain sizes ~ 1 μm but tetragonal splitting is only visible in the fluxed case. The stoichiometric sample and the 3% BaO excess have similar peak shape – the additional asymmetry in the 3% excess is attributed to the Pt 002 reflection.

To bring this data into the context of previous work, it is necessary to divide the observations into two categories: 1) the observation of a large solubility window, and 2) the ability for Ba excess to promote grain growth. For many years the available data suggested that the solubility limit of BaO in $BaTiO_3$ was limited to the 100 ppm range, however, a recent body of work by Lee *et al.* has clearly shown that BaO can be accommodated – at equilibrium – to the 1.15% range[15,16,18]. This new window was identified by calorimetric measurements of the composition dependence of the tetragonal-to-cubic phase transition. This 1 % solubility range is certainly smaller than the 4% metastable range that we observe, however, the volume fraction of material that precipitates from the films at 1200 °C for 5% Ba excess indicates that roughly 1% of material remains in solution. Though this calculation is rough, it is in agreement with the reports of Lee and the report of Hong who also observed solubility to the 1% BaO excess range[16,50]. The authors further note that 1200 °C Ba excess samples were prepared on Ni substrates and gave identical results to Pt despite the strongly reducing atmosphere during firing (10^{-14} atm pO_2). This result is again in agreement to Lee *et al*. who found minimal solubility dependence to the solubility window[16].

With regard to the microstructural implication of nonstoichiometry, the authors can only speculate regarding mechanisms. It is useful, however to begin with the literature reports that though few in number indicate that $BaTiO_3$ with excess BaO show reduced grain growth[51,52]. This observation is contradictory to the present findings, however, the ranges of grain size are quite different. It is important to

remember that Kulcsar found reduced grain size: from ~ 10 μm grains in 1:1 $BaTiO_3$ to ~ 2 μm if 1% BaO excess was introduced. In the current study we find substantial grain growth with > 2% BaO excess, but this grain growth spans the conventional thin film range of 50 to 100 nm to ~ 1 μm.

We speculate that the mechanism of grain growth is solid-state diffusion that is enhanced by metastable solubility. Since rapid grain growth is not observed at a BaO excess of 2% (which is larger than the equilibrium window determined by Lee *et al.*) the additional metastable accommodation of BaO is believed to have provided the additional defects that facilitate transport and grain growth. The possible mechanism is based on the creation of vacant titanium sites, which should enhance overall transport given the relative slowness of Ti diffusion and its participation as the rate limiting species[53,54].

4.6 Conclusions

By preparing $BaTiO_3$ thin films from metalorganic precursor solutions with large excess quantities of BaO, the authors realize a new avenue for enhancing grain growth in perovskite thin films. The results suggest that with BaO excess of greater than 2 mol % and a final processing temperature of 1060 °C, average grain sizes of ~ 0.8 μm can be achieved in thin films with 0.7 μm thickness. This yields a material with a room temperature permittivity and loss tangent values of 4000 and 0.06 at room temperature. These values are consistent with the very best reports of bulk $BaTiO_3$. The

excess BaO produces dramatic grain growth and is observed with metastable solubility approaching 5 mol %. Sufficiently high deviations in stoichiometry and annealing temperatures collapse this solubility, but microstructural and crystallographic analysis suggests that the final $BaTiO_3$ phase contains approximately 1% BaO excess. Though the observations of metastable solubility are unprecedented, the data suggests that equilibrium compositions are comparable to recent reports of Lee *et al.* The mechanisms are unclear, but the authors propose a solid-state mechanism that is facilitated by high Ti-site vacancy populations. At this stage of development, the impact of stoichiometry deviations on transport and reliability are unclear, but despite this uncertainty, this data projects new opportunities for engineering thin film grain structure without the aid of second phases or sintering aids.

4.7 References

[1] W. J. Borland, Personal communication.

[2] K. Saegusa, Japanese Journal of Applied Physics Part 1-Regular Papers Short Notes & Review Papers **36,** 6888-6893 (1997).

[3] Q. Zou, H. E. Ruda, and B. G. Yacobi, Applied Physics Letters **78,** 1282-1284 (2001).

[4] J. F. Ihlefeld, W. J. Borland, and J. P. Maria, Advanced Functional Materials **17,** 1199-1203 (2007).

[5] M. D. Losego, L. H. Jimison, J. F. Ihlefeld, and J. P. Maria, Applied Physics Letters **86,** - (2005).

[6] J. P. Maria, K. Cheek, S. Streiffer, S. H. Kim, G. Dunn, and A. Kingon, Journal of the American Ceramic Society **84,** 2436-2438 (2001).

[7] P. Daniels, J. Ihlefeld, W. Borland, and J. P. Maria, Journal of Materials Research **22,** 1763-1766 (2007).

[8] K. Kinoshita and a. Yamaji, Journal of Applied Physics **47,** 371-373 (1976).

[9] J. F. Ihlefeld, A. M. Vodnick, S. P. Baker, W. J. Borland, and J. P. Maria, Journal of Applied Physics **103,** - (2008).

[10] S. M. Aygun, P. Daniels, W. Borland, and J. P. Maria, Journal of Applied Physics **103,** - (2008).

[11] M. H. Frey and D. A. Payne, Physical Review B **54,** 3158-3168 (1996).

[12] M. H. Frey, Z. Xu, P. Han, and D. A. Payne, Ferroelectrics **206,** 337-353 (1998).

[13] J. F. Ihlefeld, (2006), *Synthesis and Properties of Barium Titanate Solid Solution Thin Films Deposited on Copper Substrates,* NCSU dept. of MSE., PHD thesis

[14] J. Ihlefeld, B. Laughlin, A. Hunt-Lowery, W. Borland, A. Kingon, and J. P. Maria, Journal of Electroceramics **14,** 95-102 (2005).

[15] S. Hoffmann and R. Waser, Journal of the European Ceramic Society **19,** 1339-1343 (1999).

[16] C. B. Parker, J. P. Maria, and A. I. Kingon, Applied Physics Letters **81,** 340-342 (2002).

[17] I. Barin, *Thermochemical data of pure substances* (VCH, Weinheim, Federal Republic of Germany; New York, NY, USA, 1989).

[18] T. M. Shaw, S. Trolier-McKinstry, and P. C. McIntyre, Annual Review of Materials Science **30,** 263-298 (2000).

[19] L. J. Sinnamon, M. M. Saad, R. M. Bowman, and J. M. Gregg, Applied Physics Letters **81,** 703-705 (2002).

[20] Y. H. Hu, M. P. Harmer, and D. M. Smyth, Journal of the American Ceramic Society **68,** 372-376 (1985).

[21] S. Lee, C. A. Randall, and Z. K. Liu, Journal of the American Ceramic Society **90,** 2589-2594 (2007).

[22] S. Lee, Z. K. Liu, M. H. Kim, and C. A. Randall, Journal of Applied Physics **101,** - (2007).

[23] T. F. LIN, C. T. Hu, and I. N. Lin, Journal of the American Ceramic Society **73,** 531-536 (1990).

[24] F. Kulcsar, Journal of the American Ceramic Society **39,** 13-17 (1955).

[25] C. Q. Tang and S. Yao, Crystal Research and Technology **35,** 609-614 (2000).

[26] G. V. Lewis and C. R. a. Catlow, Radiation Effects and Defects in Solids **73,** 307-314 (1983).

[27] R. Wernicke, Philips Research Reports **31,** 526-543 (1976).

Chapter 5: Conclusions

The work presented in this thesis was based upon the idea of achieving a thin film capacitor on foil technology that would meet commercial needs. Such a technology requires a very large area electrode and high permittivity to be able to replace bulk ceramic capacitors with the intended embedded capacitor technology. This thesis addressed both electrode are and dielectric permittivity and produced several important results:

- A novel co-firing process was developed that allowed for the production of ultra-large area electrodes without requiring a clean room environment. The surface area of thin film capacitors with yield above 75% increased by more than 4 orders of magnitude.
- The mechanism associated with the new co-firing process was explained. The difference in surface energy between the dielectric and the top electrode causes the electrode metal to retreat from areas of low radius of curvature. The advantages of this mechanism may be applied to other systems in the future.
- The effects of the A to B site ratio in Barium Titanate thin films was explored. It was found that the solubility of barium in thin film barium titanate is much higher than that of bulk barium titanate.

- It was also found that large amounts of excess barium (around 3%) provided a mechanism for large grain growth in thin films. Grain sizes in excess of 5 microns were produced in films with thickness of 1 micron.
- The grain sizes observed were also found to contribute to a much higher room temperature permittivity than has ever before been seen in thin films of barium titanate on base metal foils. A room temperature permittivity of 4000 was observed for a 1 micron thick film on copper foil with 3% excess barium that showed no presence of secondary phases.

References

[1] W. J. F. Borland, S., in Circuitree (2001).

[2] L. e. a. Wan, Electronic Components and Technology**,** 1617-1622 (2005).

[3] R. T. e. a. Croswell, Circuitree (2002).

[4] J. P. Maria, K. Cheek, S. Streiffer, S. H. Kim, G. Dunn, and A. Kingon, Journal of the American Ceramic Society **84,** 2436-2438 (2001).

[5] G. Arlt, D. Hennings, and G. Dewith, Journal of Applied Physics **58,** 1619-1625 (1985).

[6] M. H. Frey and D. A. Payne, Physical Review B **54,** 3158-3168 (1996).

[7] E. a. Little, Physical Review **98,** 978-984 (1955).

[8] W. J. Merz, Physical Review **75,** 687-687 (1949).

[9] a. J. Bell, a. J. Moulson, and L. E. Cross, Ferroelectrics **54,** 487-490 (1984).

[10] M. H. Frey, Z. Xu, P. Han, and D. A. Payne, Ferroelectrics **206,** 337-353 (1998).

[11] H. N. e. a. Al-Shareef, Integrated Ferroelectrics 3**,** 321-332 (1993).

[12] P. D. R. Hren, S. H.; Al-Shareef, H. N.; Ameen, M. S.; *Vol. ADP006688* (1991), p. 15.

[13] J. F. Ihlefeld, A. M. Vodnick, S. P. Baker, W. J. Borland, and J. P. Maria, Journal of Applied Physics **103,** - (2008).

[14] D. E. Rase and R. ROY, Journal of the American Ceramic Society **38,** 102-113 (1955).

[15] Y. H. Hu, M. P. Harmer, and D. M. Smyth, Journal of the American Ceramic Society **68,** 372-376 (1985).

[16] S. Lee, C. A. Randall, and Z. K. Liu, Journal of the American Ceramic Society **90,** 2589-2594 (2007).

[17] K. H. Hardtl and R. Wernicke, Solid State Communications **10,** 153-& (1972).

[18] S. Lee, Z. K. Liu, M. H. Kim, and C. A. Randall, Journal of Applied Physics **101,** - (2007).

[19] a. Beauger, J. C. Mutin, and J. C. Niepce, Journal of Materials Science **19,** 195-201 (1984).

[20] M. S. Mohammed, R. Naik, J. V. Mantese, N. W. Schubring, A. L. Micheli, and A. B. Catalan, Journal of Materials Research **11,** 2588-2593 (1996).

[21] R. C. Pullar, Y. Zhang, L. F. Chen, S. F. Yang, J. R. G. Evans, P. K. Petrov, A. N. Salak, D. A. Kiselev, A. L. Kholkin, V. M. Ferreira, and N. M. Alford, Journal of the European Ceramic Society **27,** 4437-4443 (2007).

[22] S. K. Streiffer, C. Basceri, C. B. Parker, S. E. Lash, and A. I. Kingon, Journal of Applied Physics **86,** 4565-4575 (1999).

[23] S. Stemmer, S. K. Streiffer, N. D. Browning, and A. I. Kingon, Applied Physics Letters **74,** 2432-2434 (1999).

[24] R. W. Schwartz, Chemistry of Materials **9,** 2325-2340 (1997).

[25] M. P. Siegal, P. G. Clem, J. T. Dawley, J. Richardson, D. L. Overmyer, and T. G. Holesinger, Journal of Materials Research **20,** 910-921 (2005).

[26] S. Hoffmann and R. Waser, Journal of the European Ceramic Society **19,** 1339-1343 (1999).

[27] J. F. Ihlefeld, Synthesis and Properties of Barium Titanate solid solution thin films on copper substrates, (2006), p. xx, 250 p.

[28] B. J. Laughlin, Sputtered $(Ba_{-x}Sr_{1-x})TiO_3$, BST, thin films on flexible copper foils for use as a non-linear dielectric, (2006), p. xxv, 232 p.

[29] D. Ghosh, Tunable Microwave Devices using BST (barium strontium titanate) and base metal Electrodes, (2005), p. xv, 188 p.

[30] B. Laughlin, J. Ihlefeld, and J. P. Maria, Journal of the American Ceramic Society **88,** 2652-2654 (2005).

[31] T. Horikawa, N. Mikami, T. Makita, J. Tanimura, M. Kataoka, K. Sato, and M. Nunoshita, Japanese Journal of Applied Physics Part 1-Regular Papers Short Notes & Review Papers **32,** 4126-4130 (1993).

[32] N. K. Pervez, P. J. Hansen, and R. A. York, Applied Physics Letters **85,** 4451-4453 (2004).

[33] D. P. Cann, Thesis (Ph.D.), Thermochemical interactions at electrode interfaces in electroceramic applications, Thesis, Pennsylvania State University., 1997.

[34] D. Chatain and W. C. Carter, Nature Materials **3,** 843-845 (2004).

[35] M. Mclean and E. D. Hondros, Journal of Materials Science **6,** 19-& (1971).

[36] J. Ihlefeld, B. Laughlin, A. Hunt-Lowery, W. Borland, A. Kingon, and J. P. Maria, Journal of Electroceramics **14,** 95-102 (2005).

[37] R. W. Schwartz, T. Schneller, and R. Waser, Comptes Rendus Chimie **7,** 433-461 (2004).

[38] W. J. Borland, Personal communication.

[39] K. Saegusa, Japanese Journal of Applied Physics Part 1-Regular Papers Short Notes & Review Papers **36,** 6888-6893 (1997).

[40] Q. Zou, H. E. Ruda, and B. G. Yacobi, Applied Physics Letters **78,** 1282-1284 (2001).

[41] J. F. Ihlefeld, W. J. Borland, and J. P. Maria, Advanced Functional Materials **17,** 1199-1203 (2007).

[42] M. D. Losego, L. H. Jimison, J. F. Ihlefeld, and J. P. Maria, Applied Physics Letters **86,** - (2005).

[43] P. Daniels, J. Ihlefeld, W. Borland, and J. P. Maria, Journal of Materials Research **22,** 1763-1766 (2007).

[44] K. Kinoshita and a. Yamaji, Journal of Applied Physics **47,** 371-373 (1976).

[45] S. M. Aygun, P. Daniels, W. Borland, and J. P. Maria, Journal of Applied Physics **103,** - (2008).

[46] C. B. Parker, J. P. Maria, and A. I. Kingon, Applied Physics Letters **81,** 340-342 (2002).

[47] I. Barin, *Thermochemical data of pure substances* (VCH, Weinheim, Federal Republic of Germany; New York, NY, USA, 1989).

[48] T. M. Shaw, S. Trolier-McKinstry, and P. C. McIntyre, Annual Review of Materials Science **30,** 263-298 (2000).

[49] L. J. Sinnamon, M. M. Saad, R. M. Bowman, and J. M. Gregg, Applied Physics Letters **81,** 703-705 (2002).

[50] T. F. LIN, C. T. Hu, and I. N. Lin, Journal of the American Ceramic Society **73,** 531-536 (1990).

[51] F. Kulcsar, Journal of the American Ceramic Society **39,** 13-17 (1955).

[52] C. Q. Tang and S. Yao, Crystal Research and Technology **35,** 609-614 (2000).

[53] G. V. Lewis and C. R. a. Catlow, Radiation Effects and Defects in Solids **73,** 307-314 (1983).

[54] R. Wernicke, Philips Research Reports **31,** 526-543 (1976).